THESIS FOR THE DEGREE OF LICENTIATE OF ENGINEERING

Practical Implementation of Quality Assurance Guidelines for Hyperthermia Therapy

Mattia De Lazzari

Department of Electrical Engineering
Chalmers University of Technology
Gothenburg, Sweden, 2023

Practical Implementation of Quality Assurance Guidelines for Hyperthermia Therapy

Mattia De Lazzari

Copyright © 2023 Mattia De Lazzari
All rights reserved.

Technical Report No.
ISSN
This thesis has been prepared using LaTeX.

Department of Electrical Engineering
Chalmers University of Technology
SE-412 96 Gothenburg, Sweden
Phone: +46 (0)31 772 1000
www.chalmers.se

Printed by Chalmers Reproservice
Gothenburg, Sweden, December 2023

To my family.

Abstract

Hyperthermia therapy (HT) has been proven to be a potent enhancer of chemotherapy and radiotherapy in numerous clinical trials. The effectiveness of HT is strictly dependent on the administered thermal dose, which, in turn, is dependent on the quality of the therapeutic heat applied to the patient. Quality Assurance (QA) protocols in HT exist to ensure that heating devices can consistently deliver controlled, reproducible, and high-quality treatments.

The physical characterization of HT devices requires specific procedures and instrumentation as well as adequate tissue-mimicking phantoms to perform QA experimental procedures. However, the implementation of QA guidelines is hampered due to the unavailability of suitable phantom materials and limited equipment for the QA experimental evaluation. This work addresses these gaps by (i) proposing the design of tissue-mimicking materials for routine use in HT QA procedures and (ii) demonstrating the practical implementation of the latest QA guidelines for both superficial and deep HT.

A novel fat-mimicking material was developed to mimic superficial fatty tissue. This fat phantom is based on an ethylcellulose stabilized glycerol in oil emulsion and is intended to be used in superficial HT QA procedures. Measured dielectric and thermal properties were consistent with fatty tissue properties, with an acceptable variability in most of the frequency range used in HT. This fat-mimicking material was then used in the experimental implementation of HT guidelines. The physical characterization of a superficial HT device (Lucite Cone Applicator, LCA) was conducted by assessing the quality metrics defined in the HT guidelines, demonstrating acceptable performance. These findings were further validated through computational studies.

For deep HT, a comparative study engaged six HT centers across Europe to assess the performance of commonly used deep regional heating devices. Preliminary results in experimental phantoms showed a good performance in terms of device heating capability and steerability. This study provided practical insights into implementing QA guidelines involving phantom properties, experimental setup, temperature acquisition, and time constraints. We are positive this research will benefit the routine implementation of deep HT guidelines in a clinical setting.

Keywords: Hyperthermia, quality assurance, tissue-mimicking phantoms

List of Publications

This thesis is based on the following publications:

[A] **Mattia De Lazzari**, Anna Ström, Laura Farina, Nuno P Silva, Sergio Curto, Hana Dobšíček Trefná , "Ethylcellulose-stabilized fat-tissue phantom for quality assurance in clinical hyperthermia". Published in International Journal of Hyperthermia, May. 2023.

[B] Carolina Carrapiço-Seabra, **Mattia De Lazzari**, Abdelali Ameziane, Gerard C van Rhoon, Hana Dobšícek Trefná, Sergio Curto, "Application of the ESHO-QA guidelines for determining the performance of the LCA superficial hyperthermia heating system". Published in International Journal of Hyperthermia, Oct. 2023.

Other publications by the author, not included in this thesis, are:

[C] **Mattia De Lazzari**, Fredrik Lorentzon, Anna Ström, Hana Dobšíček Trefná, "An EC-based oleogel fat-phantom for Quality Assurance procedures". *13th International Congress of Hyperthermic Oncology*, Digital, Oct. 2021.

[D] **Mattia De Lazzari**, Martin Wadepohl, Hana Dobšíček Trefná, "Hyperthermia system development in the perspective of the European Medical Devices Regulation". *34th Annual Meeting European Society for Hyperthermic Oncology (ESHO)*, Göteborg, Sept. 2022.

[E] **Mattia De Lazzari**, Wojtek Napieralski, Thien Nguyen, Anna Ström, Hana Dobšíček Trefná, "Design and manufacture procedures of phantoms for hyperthermia QA guidelines". *Proc. 17th European Conference on Antennas and Propagation (EuCap)*, Florence, Italy, Mar. 2023.

[F] **Mattia De Lazzari**, Dario Rodrigues, Sergio Curto, Carolina C. Seabra, Dietmar Marder, Hana Dobšíček Trefná, "Supporting the design of QA phantoms for deep hyperthermia devices". *35th Annual Meeting European Society for Hyperthermic Oncology (ESHO)*, Köln, Sept. 2023.

[G] **Mattia De Lazzari**, Carolina C. Seabra, Dietmar Marder, Sergio Curto, Hana Dobšíček Trefná, "Design of a multi-institutional study on Deep Hyperthermia QA assessment". *35th Annual Meeting European Society for Hyperthermic Oncology (ESHO)*, Köln, Sept. 2023.

Acknowledgments

I want to express my heartfelt gratitude to my supervisor, Prof. Hana Dobšíček Trefná, for her invaluable and resolved support. Thank you for believing in me, especially during times when I doubted myself. Additionally, I sincerely appreciate Dr. Dario Rodrigues, my co-supervisor, for his valuable guidance, even remotely.

I am grateful to all my current colleagues in the biomedical electromagnetics group: Laura, Moein, Alejandra, Robin, August, Andreas, Xuezhi, and Mikael. A special acknowledgment to Laura and Moein for being exceptional friends in these three years. Thank you guys for sharing the ups and downs.

During my time at Chalmers, I've been (and still am) fortunate to be surrounded by fantastic people who have become cherished friends. Naming all of you would be impossible for the sake of space, but I can still mention some. Thank you, Gabriel, Rita, Albert, Attila, Alejandra, and many more.

I sincerely thank my friends here in Göteborg – Brett, Hans, Alexia, Hampus, Arman, Anna, Henry, Lucas, Andrea, Chiara, and all the others. You've made Sweden feel like a second home.

I appreciate the Hyperboost community for sharing this project, with special thanks to Carolina Seabra for being such a good colleague.

To my friends back in Italy – the group from Piombino Dese and university friends – a special thanks. Especially to my dear friends Davide and Elisabetta, distance hasn't diminished our connection.

Finally, I have immense gratitude to my family for their unwavering support and love from Italy to here. Grazie mamma, papà, Marco, Ale, zie, zii e nonni. Vi voglio bene.

Mattia, Göteborg, December 2023

Acronyms

HT:	Hyperthermia
QA:	Quality Assurance
LCA:	Lucite Cone Applicator

RT:	Radiotherapy
EM:	Electromagnetic

Contents

Abstract i

List of Papers iii

Acknowledgements v

Acronyms v

I Overview 1

1 Introduction 3

2 Hyperthermia Principles 7

2.1 Interaction of ionizing and non-ionizing radiation with tissues . 7

Applications of radiation in oncology 9

2.2 Biological effects of hyperthermia temperatures 10

2.3 Thermal dose 13

2.4 Hyperthermia Delivery 15

Superficial HT 16

Deep HT 18

Interstitial and intracavitary HT 18

Whole body HT 19
HT systems architecture 19
2.5 Adverse effects associated with RT and HT 20

3 Quality Assurance Protocols 23
3.1 QA in Radiotherapy: an overview 24
3.2 Hyperthermia QA guidelines 26
Instrumentation and operating conditions for QA procedures . 28
Requirements for HT equipment 30
Superficial HT QA guidelines 31
Deep HT QA guidelines 33
3.3 QA phantoms development 34
Ethylcellulose based fat phantom for superficial HT 37
Deep HT QA phantoms 41

4 Hyperthermia QA protocols: experimental implementation 47
4.1 Superficial HT QA assessment 47
Experimental procedure 48
Results of the numerical validation 50
Challenges in the superficial HT guidelines application 51
4.2 Deep HT QA assessment 53
Study design 53
Observations and points of attention 55

5 Summary of included papers 61
5.1 Paper A 61
5.2 Paper B 62

6 Concluding Remarks and Future Work 65

References 69

II Papers 85

A Fat-mimicking Phantom A1

B LCA QA B1

Part I

Overview

CHAPTER 1

Introduction

Cancer is reported by the World Health Organization (WHO) as a prominent global cause of death, responsible for approximately 10 million fatalities in the year 2020 [1]. This devastating illness is an umbrella term encompassing diseases capable of afflicting virtually any part of the human body. A key aspect of cancer involves the accelerated generation of abnormal cells that proliferate beyond their usual confines. These cells can subsequently infiltrate neighboring body regions and disseminate to distant organs, a phenomenon known as metastasis. It is primarily the extensive metastatic spread of cancer that constitutes the principal underlying cause of mortality associated with cancer [2].

Figure 1.1 illustrates the incidence of new cases for the most prevalent cancer types in 2020 and their corresponding mortality rates. Leading the list in terms of mortality are lung, colorectal, and liver tumors. However, due to advancements in diagnostic techniques and more efficient treatment modalities, mortality rates have consistently decreased since the early '90s for most common cancer types, including lung, colorectal, breast, and prostate cancers [3].

In contemporary oncology, the standard treatment options include surgery,

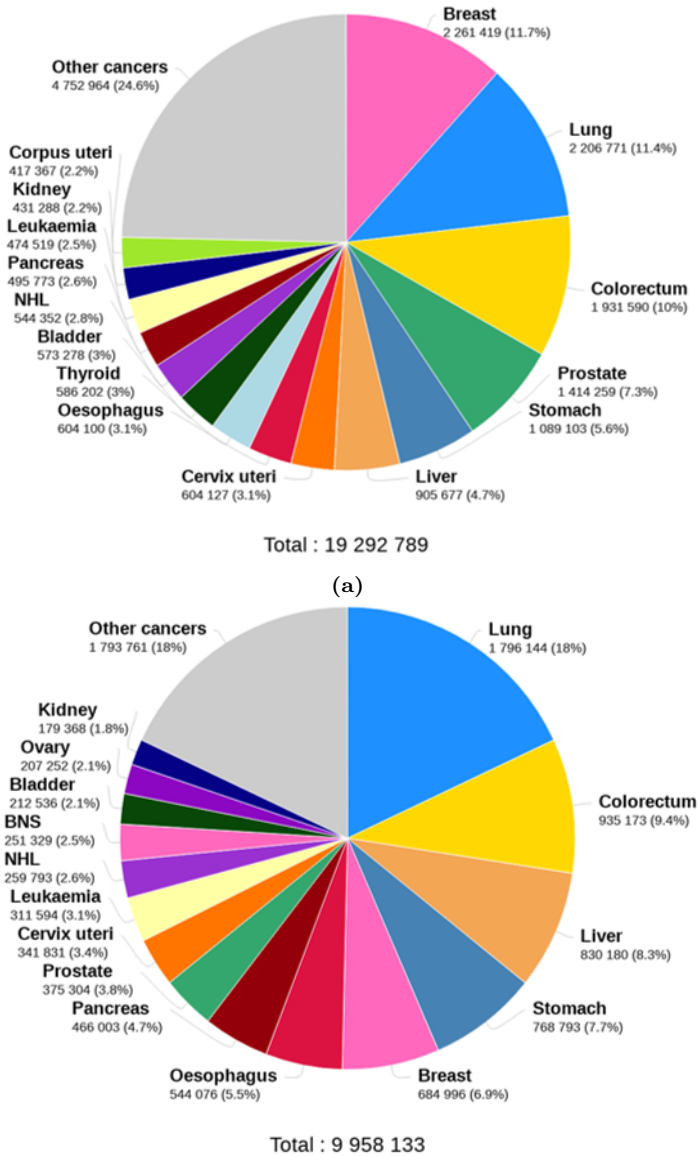

Figure 1.1: **(a)** Global incidence of the most common cancer types worldwide in 2020; **(b)** Death cases for the same cancer types as in **(a)**, worldwide, in 2020. Data retrieved from [1]

radiotherapy, and chemotherapy. These treatment modalities can be delivered as individual therapies or combined. More recent modalities include hormone therapy, anti-angiogenic treatments, stem cell therapies, and immunotherapy [4].

Surgery is often the first choice for cancer treatment, but it is common to add other therapies to enhance the probability of tumor control. Radiotherapy (RT), involving the targeted delivery of ionizing radiation to the tumor, is highly effective but adds various site-specific adverse effects and systemic reactions. Chemotherapy, which employs one or more anti-cancer drugs, exhibits varying efficacy depending on the cancer type and stage. Still, it leads to systemic reactions due to the systemic circulation of the chemotherapeutic drugs.

Hyperthermia therapy (HT) is acknowledged as a powerful adjunct to established cancer treatment techniques, significantly enhancing the effectiveness of both RT and chemotherapy [5], [6]. HT is defined by a local temperature elevation, targeting cancerous tissue within 40-44°C for one hour.

The potential of HT as a biological sensitizer has been extensively validated in many clinical trials when added to RT and/or chemotherapy [7]–[13]. Hyperthermia has demonstrated enhanced local tumor control, improved progression-free survival, and overall survival for various cancer types, including breast [7], [14], rectum [15], cervix [16], [17], esophagus [18], head and neck [19], sarcoma [20], and melanoma [21].

While numerous positive clinical trials support the efficacy of hyperthermia in treatment, two specific studies [22] demonstrated that inadequate heating administration during treatment could result in no benefit. Furthermore, several studies have found a direct and positive correlation between the administered thermal dose and clinical outcomes [23]–[28], where thermal dose is a clinical measure that combines the achieved temperature in tissue and heating duration.

The results presented in references [28] and [25] are particularly relevant for the large patient cohort considered, focusing on breast and cervix cancer. Bakker et al. [25] investigated 2,330 patients undergoing combined RT and HT for recurrent breast cancer. This study revealed that, on average, patients receiving a high thermal dose achieved a 34% higher complete response rate than those receiving a low thermal dose, without an increase in treatment-related toxicity. Similar results have been shown for cervix carcinomas by

Kroesen et al. [28].

The primary reason behind sub-optimal heat delivery can be traced to the inefficiency of HT devices, as they fail to deliver the required thermal dose and insufficient treatment monitoring and control. Quality assurance (QA) guidelines play a pivotal role in averting these deficiencies by prescribing robust and well-defined protocols that enable (a) systematic management of the treatment process from the planning phase to results documentation, (b) comprehensive characterization of the heating capacity of the applicators, and (c) assurance of adequate safety measures for both patients and healthcare personnel. The most recent version of QA guidelines for clinical HT include superficial [29], [30], interstitial [31], and deep [32], [33] applications.

This thesis focuses on assessing the heating capabilities of HT devices, which requires the deployment of specialized procedures and instrumentation such as tissue-mimicking phantoms designed to accurately mimic the properties of human tissues. The successful implementation of QA guidelines faces several challenges, including the unavailability of appropriate phantom materials and a limited experimental feasibility assessment. As such, this thesis aims to overcome these limitations by proposing the design of effective phantom materials to allow a systematic evaluation of HT equipment and demonstrating the practical implementation and eventual shortcomings of current QA guidelines.

The structure of the thesis is organized as follows. Chapter 2 presents an overview of HT, covering its biological effects and various treatment delivery modalities. This chapter also emphasizes the inherent risks associated with HT, drawing parallels with RT. Chapter 3 focuses on the latest QA guidelines for clinical HT, elucidating the fundamental principles governing the design of phantoms tailored for QA procedures. Particular focus is directed toward the design of a fat-mimicking phantom for superficial HT and phantoms suitable for deep HT applications. Chapter 4 elucidates the practical implementation of QA guidelines for both superficial and deep HT, providing a practical guide for these processes. A concise summary of the included research papers is offered in Chapter 5. Finally, Chapter 6 includes concluding remarks and a discussion of perspectives for future research.

CHAPTER 2

Hyperthermia Principles

Electromagnetic (EM) radiation manifests as energy traveling through a medium in the form of waves or energized particles. The EM spectrum includes a wide range of EM frequencies with characteristic behaviors within certain ranges. Progressing by wavelength, this spectrum includes radio waves, microwaves, infrared radiation, visible light, ultraviolet radiation, X-rays, and gamma rays. The energy conveyed by an EM wave exhibits an inverse relationship with its wavelength. Depending on the energy carried by the wave, one of the fundamental classifications is based on its ability to ionize atoms and molecules. We can then distinguish between ionizing and non-ionizing radiation, which have various applications in the medical field.

2.1 Interaction of ionizing and non-ionizing radiation with tissues

Radio waves and microwaves, generally considered harmless, are located on the lower energy radiation spectrum. These are labeled as non-ionizing radiation, as their energy levels are insufficient to initiate the ionization process within

the medium they traverse, precluding the emission of electrons from atoms. The non-ionizing radiation includes wavelengths longer than 100 nm [34].

Ionizing radiation, in turn, is characterized by shorter wavelengths and higher energy levels. Upon interaction with tissues, ionizing radiation transfers a specific amount of energy to the tissue. A straightforward method for quantifying the radiation dosage to a particular tissue volume is through the fundamental dose, denoted as D, and defined as follows:

$$D = \frac{d\bar{\epsilon}}{dm} \tag{2.1}$$

where d$\bar{\epsilon}$ represents the average amount of energy delivered to a given mass dm by the ionizing radiation. The absorbed dose is measured in joules per kilogram (J$\cdot kg^{-1}$), typically described as gray (Gy).

One of the main effects of ionizing radiation when interacting with biological tissue is to induce DNA damage. Ionizing radiation has a biological impact on DNA molecules through direct and indirect mechanisms [35]. In the direct effect, ionizing radiation directly damages the DNA molecule, disrupting its molecular structure. Such structural alterations result in cellular damage or even cell death. In this context, DNA damage typically manifests as single or double-strand breaks [36]. In the indirect mechanism, radiation interacts with tissue water molecules, which release free radicals [35]. Free radicals are highly reactive due to their unpaired electrons and subsequently react with DNA molecules, inducing molecular structural damage.

Non-ionizing radiation is defined by its lower frequencies, ranging from below 100 kHz (low-frequency RF) to 750–940 THz (UV-A). This range also includes microwaves (MW) that range from 300 MHz up to 300 GHz. With frequencies beyond 30 MHz, dielectric losses are prominent in tissues, inducing heating primarily through the mechanical friction between adjacent polar water molecules oscillating in the time-varying field [37]. The energy absorbed in the human body due to exposure from RF/MW fields is quantified in terms of Specific Absorption Ratio (SAR), derivable from the root mean square (RMS) electric field $\mathbf{E}$ as:

$$SAR = \frac{1}{V}\int_{sample} \frac{\sigma(\mathbf{r})|\mathbf{E}(\mathbf{r})|}{\rho(\mathbf{r})} d\mathbf{r} \tag{2.2}$$

where V (m^3) represents the volume of tissue considered, σ (S/m) the tissue

conductivity and ρ (kg/m^3) its density.

The energy absorbed in tissue is then converted to heat, thus inducing a temperature increase. For living biological tissues, a critical parameter that influences this temperature increase is blood perfusion, which acts as a convective heat sink. A widely recognized model that incorporates the influence of blood perfusion is the Pennes' bio-heat equation [38]:

$$c\rho\frac{\partial T}{\partial t} = \nabla \cdot (k\nabla T) - c_b W_b (T - T_b) + P \tag{2.3}$$

where k $(W/m/K)$ is the tissue thermal conductivity, c $(J/kg/K)$ is its specific heat capacity, T $(^\circ C)$ is the temperature, P (W/m^3) is the power density; c_b, w_b $(kg/s/m^3)$ are the blood heat capacity and perfusion rate, respectively; and and T_b is arterial temperature

Applications of radiation in oncology

Radiotherapy is a classic example of the use of radiation in the medical field, where ionizing radiation induces DNA damage in cancerous tissues with curative and/or palliative intent. Radiation therapy is a pivotal cancer treatment modality used in approximately 52% [39] of oncological cases. Given the potential risk to healthy tissues surrounding the target volume, the primary goal of RT treatments is to optimize the radiation dose delivered to the target region while minimizing harm to neighboring healthy tissues. This optimization is achieved by using advanced treatment planning methods incorporating high-resolution imaging such as magnetic resonance (MR) and computed tomography (CT). Additionally, fractionation techniques are used to allow healthy cells the opportunity to recover between treatment sessions.

Thermal therapies (TT) are not as widespread as RT, but they are good example of using non-ionizing radiation in medicine. TT is a broader term indicating a set of treatments based on transferring heat into or out of body tissues to accomplish a therapeutic effect [40]. Among these, EM-based TT exploit the ability of EM waves to deposit energy in tissues due dielectric loss phenomena. These elevated temperature techniques are used to treat a spectrum of illnesses, including cancer, and are divided based on the temperature range used in targe tissue: hyperthermia therapy (39-44°C) and thermal ablation (>47-50°C) [37].

Thermal ablation consists of the destruction of tissue in situ by applying

heat at high temperatures > 47-50°C for at least 10 minutes [41], [42]. This leads to irreversible effects such as protein denaturation, coagulation, necrosis, and apoptosis, with consequent complete cellular death. The energy is commonly administered through applicators (e.g. RF/MW antennas or laser fibers) inserted directly in the target organ [43], [44].

Hyperthermia therapy (HT), on the other hand, uses moderate temperature levels where the goal is to heat the tumor between 40 and 44 °C [37] for 60 minutes. Both hyperthermic and ablation temperatures induce a plethora of biological effects, further detailed in section 2.2.

2.2 Biological effects of hyperthermia temperatures

The application of heat within the HT temperature range triggers a wide array of direct and indirect effects that enhance the sensitivity of tumor cells to other firmly established treatments, such as chemotherapy and radiotherapy [45], [46]. The documented biological mechanisms induced by hyperthermia can be found in the literature [47], [48].

The direct and sensitizing effects of hyperthermia are critically dependent on the temperature reached in the targeted region and the duration of heating, as summarized in Figure 2.1. The dependency of hyperthermia effects on temperature and time has been demonstrated by in vitro studies, where increased cell death and the inhibition of DNA damage repair mechanisms when cells are exposed to high temperatures for extended periods were observed [49].

Hyperthermia temperatures above 39°C trigger a physiological response, leading to increased perfusion and enhanced vessel permeability, thereby determining changes in the tumor microenvironment. This results in improved pH levels and oxygenation, enhancing sensitivity to radiation-induced damage [50]. In vivo observations have indicated reduced tumor oxygenation and vascular damage for temperatures exceeding 44°C. At a microscopic level, high temperatures lead to an increase in the fluidity of proteins and lipids in the cell membrane. This results in heightened permeability to certain molecules, including chemotherapeutic agents.[51]. Furthermore, increased blood flow facilitates the recruitment of immune cells from lymphatic nodes to the tumor site [52]. This, in turn, triggers an immune response stimulated by hyperthermia, with evidence supporting its effectiveness in the temperature range of

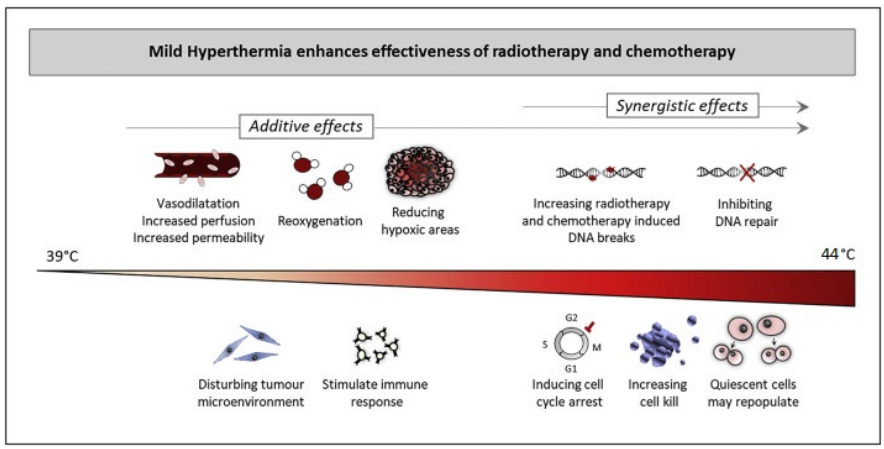

Figure 2.1: Summary of the synergetic and additive effects of hyperthermia, depending on the temperature. Adapted from [48]. Hyperthermia, up to 44 °C, induces vasodilation, enhancing blood perfusion for deeper penetration of chemotherapeutic agents. This increased permeability boosts oxygenation, intensifies radiation-induced DNA breaks, and reduces tumor hypoxic areas, altering the microenvironment and stimulating immune responses. Additionally, mild hyperthermia amplifies residual DNA breaks, promoting cell cycle arrest and making cells more susceptible to radiotherapy and hyperthermia, especially if temperatures exceed 41°C, as it inhibits DNA repair.

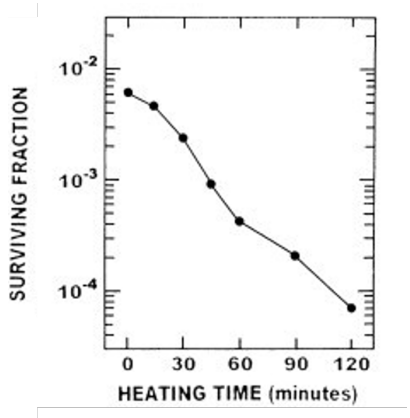

Figure 2.2: Response of HA-1 cells to irradiation with 12 Gy and then immediately heated at 43°C for different times. Reprinted from [5]

40°C-41°C [5], [53].

Studies have revealed that localized temperature elevation enhances the activation of cytotoxic T-cells and initiates a systemic immune response capable of targeting tumor cells located far from the heated region, a phenomenon known as abscopal effect [54]. Additionally, hyperthermia plays a pivotal role in disrupting various DNA repair pathways, inhibiting the activity of proteins crucial for mending DNA damage caused by external factors such as radiotherapy [55]. For instance, hyperthermia effectively suppresses the DNA repair mechanism known as homologous recombination [56]. Specifically, the most effective suppression of DNA repair mechanisms, including homologous recombination, is observed at temperatures exceeding 42°C with a treatment duration of 60 minutes [57].

As discussed in the previous paragraphs, the interaction of HT with radiation depends not only the temperature reached during heating but also the duration of the heating process. In Figure 2.2, the survival fraction of Chinese hamster cells is depicted after exposure to irradiation with 12 Gy, followed by immediate heating at 43°C for varying heating durations. Generally, a more prolonged exposure to elevated temperatures results in an intensified effect. However, while extended heating periods lead to lower survival of cancer cells, it also initiates a cellular response known as the heat shock response, designed

to protect against protein stress [58]. This response results in the rapid production of heat shock proteins (HSPs), leading to thermotolerance, which is reduced sensitivity to heat treatments within 48–72 hours following the initial treatment. This aspect is of great importance and emphasizes the need for precise scheduling of HT sessions for patients. Therefore, the treatment time is limited to 1.5 hours, and the treatment is never administered more than 2 times per week.

2.3 Thermal dose

Thermal therapy treatments can be quantified in terms of thermal isoeffective dose, or simply thermal dose, which represents the combined impact of temperature and treatment duration expressed in terms of an equivalent time at the reference temperature 43°C to reflect the effect of the temperature to direct cell death [59].

A standard definition for thermal dose is the cumulative equivalent minutes at 43°C (CEM43) [60], representing the effect of the entire history of heat exposure on cell death. This definition allows the comparison of HT treatments with different temperatures and heating durations. CEM43 does not take into account the radio- or chemo-sensitizing effects of heat, but it is still the most widely used metric for thermal therapy treatments, acting as a de facto standard. Following this definition, the equivalent thermal dose can be expressed as:

$$CEM43 = \sum_{t=0}^{t=t_{total}} R^{(43^{\circ}C-T)} \Delta t \tag{2.4}$$

where t_{total} is the total treatment time, Δt (min) is the take between two consecutive temperature measurements, while T(°C) is the average temperature during the interval Δt. R assumes a value of 0.25 for T $<$ 43°C and 0.5 for T $\geq$ 43°C [61], and it is based on the biphasic Arrhenius plots.

The CEM43 model, however, has limitations due to its assumption that different tissues share the same heat sensitivity and its inability to account for the radiosensitization capability of HT [62]. In response to these limitations, various variants of CEM43 have been introduced. These variants incorporate temperature indices, such as T90, T50, or T10, into the CEM43 definition,

where Tx is the tumor temperature exceeded by x% of the measured temperature points. This adaptation aims to address the heterogeneous temperature distribution observed in vivo. The resulting parameters are referred to as CEM43T90 [63].

While CEM43 and its variants capture the dominant biological effect at high temperatures, in most clinical studies, it is often noted that the actual tumor temperatures recorded are lower than the intended 43°C. Consequently, alternative parameters have been proposed over the years. Clinical outcomes are typically reported in terms of maximum(T_{max}), minimum (T_{min}), and average (T_{avg}) temperatures and more often T90, T50, or T10. These parameters are also recommended in the most recent quality assurance protocols for superficial HT [29].

The TRISE parameter is proposed in [27] as an alternative to these parameters. TRISE integrates both temperature and heating duration. However, instead of converting the recorded temperatures into equivalent minutes at a reference temperature, the T50 increase above 37 °C throughout the treatment is directly multiplied by the treatment duration. The result is then normalized to the total scheduled treatment time (set to 450 min):

$$TRISE = \frac{\sum_1^n (T_{50} - 37°C) \cdot dt}{450} \tag{2.5}$$

where dt is the treatment duration and n is the number of treatments.

In another approach by Datta et al. [64], the area under the curve above ≥39°C (AUC 39°C) for transient temperature is suggested as a simple parameter that takes into account time and temperature. This parameter offers a realistic representation of the multifactorial effects of HT across the entire temperature range and is calculated as follows:

$$AUC \geq 39°C = \sum_{n=1}^{N} \Big(\frac{T_{n-1} + T_n}{2} - 38.9 \Big) (t_n - t_{n-1}) \tag{2.6}$$

where T_n denotes the temperature at the time instant t_n.

Despite the aforementioned recommendations, consensus regarding the definition of a parameter capable of accurately representing the dose-effect relationship has not yet been achieved [65]. The main reason is likely the lack of quality thermometry, including the use of a low number of probes to measure temperature, their limited placement relative to the tumor, and the rate

of temperature acquisition. These factors substantially influence our understanding of tumor temperature coverage, so the relevance of temperature parameters is currently limited. Still, current temperature metrics are critical to promote standardization and compare the results of different clinical trials.

Contrary to radiation therapy, achieving a prescribed dose in HT is a challenge. Biological factors such as tissue heterogeneity and blood perfusion contribute to an uneven focus in the target area. Moreover, limitations in heating technologies constrain the maximum achievable temperature and the depth of tissue penetration. Therefore, evaluating the heating performance of current HT devices is essential to determine an effective dose distribution. Quality assurance protocols offer systematic procedures to assure and verify the performance of HT systems and are thus critical to maximize therapeutic effects.

Strong clinical evidence highlights an association between suboptimal heating quality and unfavorable clinical outcomes. This can be attributed to both the heating inability of HT equipment and inadequate temperature monitoring. The findings presented by Perez et al. [22] do not indicate significant improvements when using RT alone compared to RT+HT in the treatment of large superficial lesions (> 3 cm). The leading cause for this negative result is attributed to the absence of stringent guidelines for patient and tumor selection in HT clinical trials as well as the absence of rigorous QA protocols for evaluating device performance. On the other hand, evidence has emerged over the years, pointing to a positive correlation between temperature, the thermal dose delivered within the target, and clinical outcomes [23]–[27].

2.4 Hyperthermia Delivery

Different technologies are available to achieve the therapeutic temperature range HT requires [66]: 40-44°C for 1 hour. Depending on the tumor location and size, the most common HT applications are superficial HT, deep HT, interstitial HT, and intracavitary HT. When heat delivery is not concentrated on a specific target volume but administered to the entire body, we refer to this approach as whole-body HT. These delivery modalities are graphically represented in Figure 2.3e.

The HT treatment delivery can be accomplished using a variety of technologies. Among these, EM-based techniques, such as capacitive, radiative, and

infrared, as well as focused ultrasound, are the most commonly used. EM-based technologies are widely adopted due to their versatility and suitability for various anatomical sites. Ultrasound technologies find limitations arising from the high acoustic impedance of bones and intestinal gases, often resulting in patient discomfort and bone heating.

Superficial HT

Superficial HT is a technique intended for treating lesions located at a maximum depth of 4 cm from the surface. Examples of tumors treated with superficial HT include lymph node metastases of head and neck tumors, breast cancer, chest wall recurrences, and melanomas [67]. The treatment is delivered by external applicators, such as antennas, either in a single or array configuration, capacitive electrodes, or infrared lamps.

Superficial HT uses antennas in the frequency range between 400 MHz and 1 GHz due to the preferential energy deposition within 4 cm from the surface [67]. Examples of these applicators include waveguide antennas, such as the 434 MHz Lucite Cone Applicator used at Erasmus MC in Rotterdam [68], and patch antennas such as the Conformal Microwave Array (CMA) [69]. In both cases, the use of multiple antenna elements is allowed to extend the treated area.

Capacitive systems use metal electrodes operating at frequencies of 8, 13.56, or 27.12 MHz [66]. Localized heat delivery is achieved using electrodes of different dimensions, where the RF fields concentrate near the smaller electrode. However, this technique may result in excessive fatty tissue heating due to the orientation of the main electric field component perpendicular to the fat–muscle interface. [70]–[72]. This is not the case for the radiative applicators, for which the field components are parallel to the interfaces between superficial fat and muscle. The interface conditions, as per Maxwell's equations, specify that the tangential E-field remains continuous while the normal E-field component experiences a discontinuity proportionate to the dielectric properties of the two distinct tissues. This results in a considerably increased electric field within the fat tissue when utilizing capacitive systems.

Infrared HT uses infrared lamps operating above 300 GHz [66]. The penetration depth of the infrared radiation is usually less than 1 cm. Still, by using customized filters, this technology can treat lesions infiltrating up to 1.5 cm below the skin surface [73]. For deeper targets, MW and RF systems are

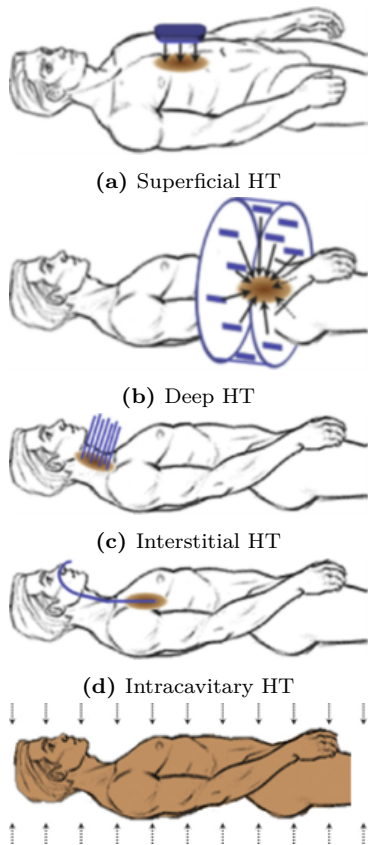

(a) Superficial HT

(b) Deep HT

(c) Interstitial HT

(d) Intracavitary HT

(e) Whole-body HT

Figure 2.3: Graphical representation of the most common HT application modalities. Reprinted from [67]

preferred.

Deep HT

Deep HT target tumors deeper than 4 cm from the skin surface. The heat is administered externally. Radiative RF and MW devices are the most commonly used, but capacitive technology is gaining traction due to the lower acquisition cost. Radiative heating of deep-seated tumors in the pelvis, such as those in the cervix, bladder, rectum, sarcoma, and pediatric tumors, has yielded exceptional clinical outcomes [12], [15], [74]–[76].

In radiative deep HT, treatment is often delivered using phased-array systems consisting of multiple antennas organized in one or more rings around the body. These systems allow power steering by adjusting the phase and amplitude settings of individual or groups of antennas. A focus in the target volume is achieved by optimizing the phase and amplitude settings to obtain constructive interference within the tumor [77], [78]. The typical frequency range used in radiative deep HT is 70-150 MHz, enabling a heating focus with a diameter of 10–15 cm [66]. Modern systems aim at smaller focus using higher frequencies and wide-band solutions [79], [80].

Capacitive devices designed for deep heating of centrally-located tumors typically feature electrodes with a diameter equal to or greater than 25 cm. However, this technique exhibits notable limitations. The uniform size of the electrodes restricts the ability to adjust the focus, thereby limiting control of the emitted power. Additionally, a substantial portion of the power is absorbed by the superficial fat layer, limiting the penetration to the desired depth. Furthermore, capacitive heating fields tend to diverge as they penetrate the body unless constrained by high-water-content pathways or restricted by low-water tissues, such as the bone structures in the pelvis. Consequently, the only way to control the shape and location of the focus is through the placement and dimensions of the electrodes used.

Interstitial and intracavitary HT

In interstitial HT, needle-shaped antennas are percutaneously inserted into the target tissue, typically operating between 500 MHz and 1.3 GHz [81]. These antenna elements have a typical active length of 4-10 cm and a diameter of 1-2 mm [40]. Various antennas have been explored to achieve interstitial

heating, including the monopole, dipole, slot, and helical coil microwave antennas [66]. Interstitial MW hyperthermia has been shown to be effective in heating tumors and achieving local control in randomized trials, mainly when used in combination with brachytherapy [82], [83].

In intracavitary HT, the antenna elements are inserted into the body via natural cavities and orifices, such as the vagina, rectum, esophagus, urethra, or bladder. The heating is primarily focused on the cavity and its immediate surroundings, reaching depths of up to 1 cm from the lumen. The applicators used in intracavitary HT are typically similar to those used in interstitial HT and have comparable active lengths but diameters up to 30 mm [67].

Whole body HT

Whole body HT uses radiant heat and infrared lamps to induce a systemic body temperature increase for a prolonged time interval. This can be achieved within the ranges of 39–40°C for 6 hours (referred to as fever-range whole body HT) or 41–42°C for 60 minutes (considered extreme whole body HT) [84], [85]. This approach is beneficial for treating distant metastases and non-solid malignancies.

HT systems architecture

As depicted in figure 2.4, generic HT systems are characterized by four fundamental blocks:

- **Signal generation and amplification unit:** Here, a signal with the desired frequency is generated by a signal generator, and power amplifiers are used to achieve the desired signal amplitude. If using a phased-array applicator, phase shifters are required to steer the focus towards the desired location.

- **Applicator:** The nature of the applicator varies depending on the specific treatment area and technology used. It can consist of antenna elements, either as single units or in an array configuration, or it may involve using infrared lamps or capacitive plates. It delivers the EM waves to the body with the required amplitude and phase. The antenna elements can be placed internally or externally on the body. When using external antenna applicators, a coupling medium is used to avoid direct

contact with the skin. Deionized water avoids field disruptions and is thus the most commonly used coupling medium, which is contained in a compartment made of plastic or skin-compatible materials. This compartment is known as the water bolus and is part of the applicator. The temperature of the water is controlled through a circulation system and offers skin cooling, preventing superficial burns.

- **Thermometry:** Essential to measure the temperature achieved in the target region or its proximity. The type of thermometry used depends on the specific application. The temperature can be measured invasively in body cavities and/or on the skin surface. Both invasive and intracavitary use catheters placed directly in the target or in its proximity. For superficial applications, the most common monitoring methods are noninvasive, which use temperature sensor arrays placed between the skin and applicator. Some centers use invasive catheters to monitor the superficial tumor more accurately since the maximum temperature can be achieved at depth. Finally, non-invasive magnetic resonance-based thermometry is another option that provides 3D temperature scans in quasi-real-time.
- **Control and treatment planning unit:** This unit is responsible for regulating the input power to the applicator and, in the case of phased array applicators, steering the signal phase according to the treatment plan. Any necessary adjustments to the antenna settings can be made automatically or manually during treatment based on the temperature measurements or measured amplitude and phase provided by a feedback loop. To date, treatments still require significant manual adjustments, and no fully automatic control unit has yet been clinically implemented.

2.5 Adverse effects associated with RT and HT

Radiotherapy treatments involve a complex process, and the associated risks are significant. The occurrence of incidents and errors in radiotherapy is estimated to be around 0.15% [86]. Approximately 40% of these incidents result in harm to patients, and in 1% of cases, the outcomes can be fatal. Furthermore, a wide range of adverse effects are expected depending on the specific treatment site. Besides DNA damage, irradiation triggers various cellular

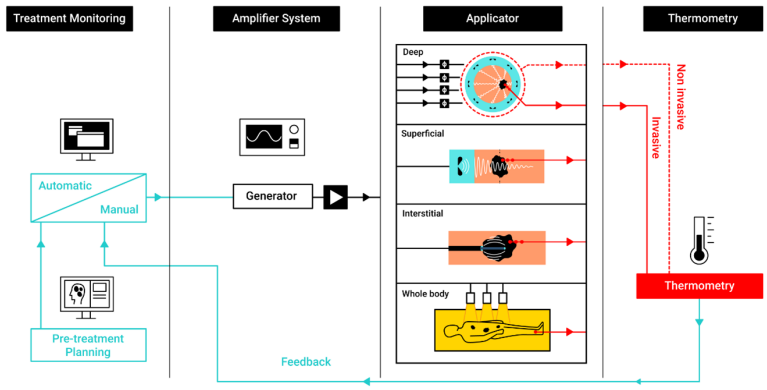

Figure 2.4: EM HT system decomposed in its main four subsystems. Different applicators are considered depending on the treatment technique.

signaling pathways, leading to the expression and activation of proinflammatory and profibrotic cytokines, coagulation cascades, and vascular injury [87]. These changes contribute to developing edema, inflammatory responses, erythema in the skin, increased intracranial pressure in the central nervous system, and lung fibrosis [88]. For example, in treatments of the abdomen and pelvis, adverse effects can manifest in the gastrointestinal tract, resulting in symptoms such as anorexia, nausea, vomiting, abdominal cramps, and diarrhea. Radiotherapy can also lead to varying degrees of irritation and functional impairment to the bladder, as well as conditions like cervicitis and vaginitis in women [88].

Systematic QA programs in RT are firmly integrated into routine practice to ensure accurate treatment delivery, minimize chances of errors and accidents, and optimize dose delivery to the target tissue to mitigate life-altering side effects. For this reason, a more comprehensive overview of these QA and safety measures is presented in the following chapter.

Hyperthermia is a therapeutic technique that exploits the application of non-ionizing radiation within the RF/MW frequency range. While not as harmful as RT, careful energy delivery to the body still requires caution, considering potential harm and side effects for the patient and medical staff. Similar to RT, the effects of HT can be categorized as direct and indirect.

A direct effect of HT involves the energy deposition to the tissue, leading to a temperature increase, the primary effect exploited in HT. However, direct effects can sometimes result in local burns, hotspots, and potential circulatory system disturbances due to attempts to cool the heated areas [89].

The indirect effects of HT encompass the generation of electric currents in conducting materials, potentially leading to burns when in contact with the current-heated material. Additionally, the EM field propagated during HT sessions might interfere with the normal functioning of other life support devices, such as pacemakers, which is in turn, a contraindication for many EM-based HT devices [90].

The direct and indirect unwanted effects of HT can be mitigated by implementing appropriate safety measures and protocols. Safety standards regarding field protection are available, such as IEEE C95.1-2019 [91] and the ICNIRP guidelines of 2020 [92]. An adequately shielded treatment room helps avoid potential harm to other devices and personnel. In general, no direct effects on the staff are expected due to the limited specific absorption rate (SAR) levels.

Well-designed QA procedures further minimize the risk to patients and users, together with, as previously discussed, assuring an uniform heat distribution.

CHAPTER 3

Quality Assurance Protocols

The term Quality Assurance (QA), as defined by the International Standard Organization (ISO), is "all those planned or systematic actions necessary to provide adequate confidence that a product or service will satisfy given requirements for quality" [93]. In the medical context, this concept translates into efforts aimed at monitoring the quality of care provided to individuals or groups of patients, enabling the identification of potential deficiencies and facilitating corrective actions. A prime illustration of this can be found in radiation oncology, where QA programs form an integral part of radiation therapy practice [94]. These programs play a pivotal role in minimizing the probability of accidents and errors enhancing the safety and comfort of patients and healthcare workers.

While not as firmly established as in RT, QA procedures for HT have been available since its early days, covering both deep and superficial treatments [22], [95]. Over the years, these guidelines have been revised reflecting the increased knowledge and technological development [96], [97] until the most recent versions for deep HT [32], [33], superficial HT [30], and interstitial HT [31] QA protocols. These guidelines aim to ensure a uniform QA and treatment control level among different institutions

They also answer the need to harmonize HT QA procedures with QA protocols in radiotherapy, as these two treatments are often delivered together within the same clinical practice.

This chapter presents an overview of the most recent QA procedures in both RT and HT. Focusing then on HT, the aim is to identify the clinical and technical requirements and explore the strategies adopted to fulfill them, such as developing tissue-equivalent materials tailored for the practical implementation of clinical guidelines.

3.1 QA in Radiotherapy: an overview

QA programs are solidly settled and well integrated into modern radiation oncology, providing one of the most compelling examples of QA assuming a primary role in clinical practice. The need for QA procedure in HT derives from several factors, with the most prominent being the need for a refined dose control: normal tissue tolerance thresholds are quite strict, and there is a high correlation between tumor response and dose delivered [98]. Additionally, the technological used in RT devices is complex [94].

An initial effort to achieve these goals can be traced back to the late 70s, with the publication of the International Commission on Radiation Units and Measurements Report, which prescribed the requirement of dose delivery precision within 5% [99]. Since then, QA protocols have evolved following the development of technology, such as integrating image-based techniques and 3D treatment planning systems.

Research has demonstrated that implementing a robust QA program in RT can impact patient survival rates in the long term [100]. The rationale for a QA program in radiotherapy is based on four fundamental aspects [101]:

1. Reducing errors in treatment planning and dose delivery to enhance remission rates and minimize the risk of complications.

2. Ensuring consistent dosimetry and treatment control across various institutions, facilitating inter-institutional comparisons.

3. Optimizing the treatment's effectiveness by fully exploiting the capabilities of modern radiotherapy technology.

4. Ensuring uniform treatment quality in developed and developing countries.

A brief overview of a general QA protocol in RT is provided in reference [102]. The main target is to meet the 5% delivery precision requirements for the prescribed dose.

In modern radiation therapy (RT), QA includes three crucial domains of treatment: clinical, physical, and technical. This comprehensive approach ensures the thorough coverage of all aspects of a typical RT treatment program, including treatment planning, beam delivery, and treatment documentation:

- **Treatment planning**: This is a complex process that involves collaboration among various specialties, such as radiation oncologists, dosimetrists, and medical physicists. QA guidelines play a pivotal role throughout the entire process, starting with the treatment prescription and continuing through planning and treatment verification:
  - Prescription: Stringent requirements are imposed for written and certified documentation.
  - Patient data acquisition: QA procedures are in place for CT and MR scans, including assessments of image quality. Patient positioning is facilitated through laser alignment.
  - Contouring and Target Volume Definition: Specific QA actions are prescribed for the treatment planning system, and a peer-review process is recommended to ensure high-quality contouring and tissue delineation.
  - Specific requirements apply to the treatment planning software. Tolerance levels of 2% are set for the source isodose distribution. Periodic verifications are mandated, ranging from daily tests for I/O device functionality to annual reference QA tests.
- **Beam delivery**: The efficacy of treatment delivery is closely linked to the functional performance of therapy equipment, which directly impacts dosimetry accuracy and the patient's received dose. QA tests are prescribed, with tolerance values and recommended frequencies varying according to their impact on the patient. Daily QA tests include laser positioning verification, while mechanical tests, such as gantry and collimator isocenter verification, are conducted monthly. Polymer gel

dosimetry may be employed to measure absorbed dose distributions with high spatial resolution [103].

- **Treatment documentation**: the recording of patient identification data, treatment planning details, and the execution of treatment is crucial. This information is documented in a patient's chart, which undergoes regular review by a multidisciplinary team during treatment and upon completion. The transfer of information is also subject to specific QA procedures, as outlined in [104].

3.2 Hyperthermia QA guidelines

Similarly to RT, QA protocols in HT are designed to ensure that heating devices can consistently deliver controlled, reproducible, and uniformly high-quality treatments. The focus extends beyond the sole capability of current devices to deliver the prescribed thermal dose. Just as in RT, QA guidelines encompass a broader spectrum, covering both clinical and physical aspects of the treatment, such as:

- **Treatment planning**: The primary goal of HT treatment planning is to maximize the SAR and/or temperature coverage within the target while minimizing energy deposition in healthy tissue. As a standard, there is a defined maximum temperature limit of 44°C in healthy tissue and 42°C in bone marrow or nervous system [33]. Thus, the computational model just matches the anatomy, applicator, and clinical setup as closely as possible. There are no mandated technical requirements for computational methods employed in HT treatment planning. However, the European Society for Hyperthermia Oncology (ESHO) has published recently guidelines for HT modeling, which should be the basis for future standards in HT [105].

- **Treatment delivery**: Accurately delivering the prescribed thermal dose requires careful patient preparation and effective treatment monitoring. These critical aspects are addressed in the QA guidelines and can be summarized in three key components:
  - Patient positioning: A high degree of positioning accuracy, within 1 cm of the modeled position during the planning phase, is required

[106]. To achieve this precision, clinical staff use side lasers and markers corresponding to the applicator edges for tailoring and adjustments.

  - Temperature monitoring: Multi-sensor probes and/or thermal mapping systems are required, while non-invasive thermometry sensors or MR-based thermometry are valuable add-ons. At least one sensor must be related to the tumor temperature. It is crucial that these sensors exhibit minimal or no interaction with the EM field, and measures must be taken to prevent self-heating phenomena caused by the probes. Thermometry equipment should meet specific requirements regarding an accuracy of ±0.2°C [30]. In cases where thermal mapping is used, a track length of at least 15 cm is recommended [32].
  - Treatment documentation: Maintaining standardized and comprehensive treatment documentation is essential, as it is a requirement for evaluating treatment effectiveness. This documentation should include patient treatment setup, HT applicators used and its settings, thermometry and power data. Standardized temperature parameters such as T90, T50, T20, maximum and mean tumor temperatures should be recorded. Additionally, any patient complains and acute toxicities observed during the treatment must be reported.

- **Requirements and characterization of equipment**: An HT system must meet certain technical requirements to effectively provide targeted heating to the treatment volume while safeguarding surrounding tissues. A reliable control of the EM radiation emitted by the antenna is critical for adequate treatment delivery. Precise requirements comprehend amplitude and phase accuracy no greater than 5% and 5°, respectively, alongside a power output with reflection under 33% [32]. Regular technical assessments and a well-defined calibration and maintenance routine are essential for QA. The efficiency and technical performance of the signal generation and steering system, along with the temperature monitoring system, can be evaluated using established measurement tools and techniques, such as power meters/couplers and standard temperature probes, among others. The physical characterization of the HT

system can be realized through the use of appropriately designed tissue-mimicking phantoms. This constitutes the primary focus of this work, which will be examined in greater detail in the following sections.

- **Staff requirements and safety**: Additional guidelines pertain to the prerequisites for HT staff and safety measures. The responsible team should ideally comprise of a well-trained physician and a medical physicist. Note that there is no current certification for hyperthermia physicists, for which many institutions use engineers with training in physics and medical sciences [107] instead of traditional medical physicists. Detailed recommendations and responsibilities for all HT treatment staff can be found in reference [108]. Establishing effective audible and visual communication with the patient is essential to receive prompt feedback and thus provide immediate intervention when necessary. Furthermore, comprehensive EM field protection measures must be put in place to safeguard both staff and patients. Regularly monitoring stray EM fields during installation and on an annual basis is crucial to ensure compliance with national standards about non-ionizing radiation exposure within the HT frequency range. Adherence to the most recent standards is recommended, such as IEEE C95.1-2019 [91] and the ICNIRP guidelines of 2020 [92].

The existing guidelines comprehensively address the clinical aspects of QA in HT, including deep [33], superficial [29], and interstitial HT [31]. These clinical aspects will not be further elaborated upon in this work. Instead, our focus is directed towards novel techniques for evaluating the performance of HT systems.

Instrumentation and operating conditions for QA procedures

The QA verification of heating devices must be consistently carried out under reproducible conditions. This requires the establishment of a common and defined experimental QA protocol. A shared prerequisite for all QA procedures is achieving thermal equilibrium with room temperature at the start of experiments. When water bolus is used as a coupling medium between the applicator and phantom, it is essential to ensure that the water circulates and remains at room temperature to prevent any disruption to the heating pattern. To guarantee reproducibility, it is crucial to ensure proper and consistent

positioning of the applicator relative to the phantom.

The minimum set of QA instrumentation required should allow proper monitoring of the temperature distribution and, specifically for deep HT systems, achieving a clear focal volume. More specifically, this includes:

- Standardized phantoms: A phantom can be generally defined as an object designed to mimic properties of a particular tissue. The geometry and composition of phantoms are closely tied to the technology being assessed, as detailed in subsequent sections. A key distinction is drawn between tissue-equivalent phantoms used to analyze spatial temperature patterns and lamp phantoms, which are used to quickly evaluate EM field symmetry and steering capabilities in deep HT applicators.

- Temperature probes: The temperature probes used in HT treatments should be verified daily for calibration within ±0.2°C. If calibration is off this threshold, then probes should be recalibrated with a standard sensor until achieving a minimum requirement of ±0.2°C. To improve temperature special resolution, there are two solutions that can be used: multi-sensor or thermal mapping probes. These contrast with stationary single-sensor probes that only provide 1 measurement point. In the thermal mapping solution, the probes are positioned inside a catheter and cyclically translated by a mechanic actuator (or manually) to cover the region of interest, which can include the tumor and surrounding tissues. the measuring direction.

- IR camera: Infrared (IR) camera: This requirement is relevant when using solid and split phantoms in superficial and interstitial HT QA. The IR camera should have a minimum resolution of 0.1°C to accurately analyze the 2D thermal distribution induced in the phantom by the HT applicator.

- Additional tool: A more quantitative evaluation of the HT applicator performance can be achieved via E-field probe measurements, which can be scanned in 3D scan tanks for 3D SAR maps or a dipole probe with high-resistance leads [109]. The antenna efficiency em terms of power reflection can be carried out with a power meter or vector network analyzer.

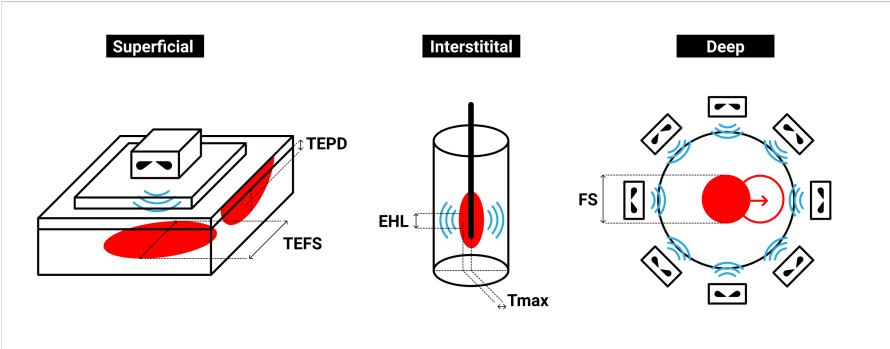

Figure 3.1: Quality metrics currently defined for the QA assessment of superficial, interstitial, and deep HT. Available from: http://www.esho.info/.

Requirements for HT equipment

This evaluation relies on well-defined parameters that are easily assessable through the use of homogeneous tissue-mimicking phantoms. Regardless of the HT technique used, a fundamental requirement for determining the suitability of a heating device for clinical HT applications is the ability to achieve a temperature rise (TR) of 6°C within a specified time frame within homogeneous tissue-mimicking phantoms. The rationale for a 6°C increase is to mimic the temperature increase during HT from core temperature (37°C) to 43°C. This criterion is further tailored to the specific HT technology under study: for superficial HT, a 6°C increase should be achieved within 6 min, at a depth of 1 cm, and in a muscle-equivalent phantom. For interstitial HT, the requirement is to achieve the same temperature rise at a distance of 0.5 cm from the applicator. For deep HT applicators, the standard is a 6°C temperature increase within 10 min for abdominal and pelvic malignancies; and 6 min for head and neck and (distal) extremities applicators. This criterion is based on previous studies [110], [111].

Furthermore, in the context of deep HT, an additional requirement is the focusing ability, which describes the ability to attain and steer a clearly defined focus within the intended treatment target volume. This can be evaluated both in terms of energy or temperature distribution, as described later.

Further technique-specific quality metrics are also accessible, primarily based on the thermal distribution established by the applicator. These are graphi-

cally summarized in Figure 3.1 and defined in the following paragraphs.

Superficial HT QA guidelines

Superficial hyperthermia is a technique intended to target lesions located within 4 cm from the skin surface [66]. Consequently, assessing the device's capability to provide effective heating in a volume close to the applicator is crucial. The ESHO QA guidelines for superficial hyperthermia [30] prescribe two quality indicators to quantify the applicator heating performance, complementary to the TR. The evaluation of these parameters is carried out using tissue-equivalent phantoms, which must accurately replicate the electrical, optical, or acoustic properties, depending on the heating technology in question, as well as the thermal properties of human tissue. The muscle-mimicking phantom is divided into different solid phantom layers to facilitate the temperature reconstruction generated by the applicator, where the layer thicknesses depend on the applicator operating frequency. The top 1 cm layer is recommended to be a fat-mimicking phantom, and the remaining layers should be a muscle-mimicking phantom. Figures 3.2a and 3.2b show the recommended configuration for frequencies under 915 MHz and above/equal to 915 MHz, respectively. The QA metrics outlined in these figures are:

- Thermal Effective Field Size (TEFS): This is defined as the area within the 50% maximum TR contour at a depth of 1 cm in a muscle-mimicking phantom, under the applicator aperture.

- Thermal Effective Penetration Depth (TEPD): This is defined as the depth at which the maximum TR is 50% of the maximum TR (i.e.,ΔT $\geq$ 3°C in 6 minutes) at a depth of 1 cm.

TEFS and TEPD have no specified minimum requirements or values for devices to be considered adequate. They serve as metrics for evaluating the heating capability of the device and define the limitation of the applicator heating abilities in terms of depth and focus size.

The 2D thermal distribution at each interface is assessed at the top surface of each layer employing the IR camera. This approach also allows for the reconstruction of the vertical thermal distribution along the phantom z-axis. Alternatively, a vertically split phantom can be used for this evaluation. An

(a) < 915 MHz

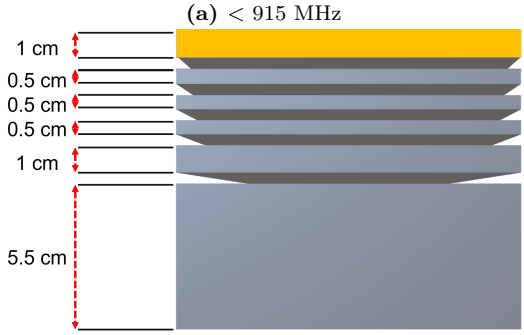

(b) ≥ 915 MHz

Figure 3.2: Phantoms for QA of superficial HT consisting of multiple fat-muscle layered mimicking phantoms. The yellow top layer represents a 1 cm thick fat phantom, whereas the remaining in gray are layers of muscle phantom

IR camera is strongly recommended due to its superior spatial resolution compared to temperature probes located at different depths within the phantom. A more detailed implementation of this procedure can be found in Chapter 4 and in Paper B.

Deep HT QA guidelines

The most recent version of QA guidelines for deep HT techniques [32] focuses on deep HT phased array systems. In these applicators, power is irradiated by a single applicator consisting of an array of equispaced and independently controlled antenna elements [67]. According to [32], the performance assessment of these applicators is based on the evaluation of the energy distribution determined by the applicator in terms of SAR, with the requirement for the ratio between SAR in the target volume (SAR_{target}) and SAR in the nontarget volume ($SAR_{non-target}$) to be at least 1.5. Other quality indicators based on SAR values are also available [112].

Updated guidelines provided by ESHO are under preparation. These new guidelines aim to shift towards a QA approach centered on temperature rather than energy-related parameters. This transition aligns with the fundamental goal of HT, which is to achieve uniform and consistent heating within a target volume while safeguarding surrounding tissues. The characterization of the applicator will be based on the assessment of temperature-based indicators, which complement the criteria related to temperature rise and focusing ability, as defined by the following metrics:

- Thermal Effective Field Volume (TEFV): refers to the volume enclosed within a homogeneous phantom that is encompassed by the 75% maximum temperature rise (TR) contour. In other words, it represents the volume where the temperature rise reaches at least 4.5°C for a target TR of 6°C.

- Focus symmetry (FSym): measures the maximum relative deviation (in percentage) of temperature rise (ΔT) between measurements taken at four equidistant points from the focus isocenter in the radial plane ($\pm$x and $\pm$y).

- Focus steering (FSteer): evaluates the applicator's ability to accurately move the isocenter of the heating region. This measurement is quanti-

fied in terms of precision (in millimeters) between the planned isocenter specified in the DHT control software and the experimental maximum temperature location determined from interpolated temperature data.

A graphical representation of these quality metrics is shown in Figure 3.3.

The experimental evaluation of these parameters is conducted on standardized phantoms, including temperature probes located at prescribed locations. These phantoms are generally made of a cylindrical hard plastic container, mimicking the external fat layer to some extent, and equipped with an internal array of catheters to allow the insertion of temperature sensors.

Phantoms equipped with LED/lamp matrices are used to assess visually the steering performance of the focus region [113]. These phantoms comprise an array of LEDs or diodes submerged in a saline solution encased within a cylindrical plastic shell. The saline solution is precisely calibrated to mimic the electrical conductivity of tissue so that the LEDs or diodes light up due to the presence of the RF field. The luminous pattern generated by the applicator is visually inspected to determine the correct focus, steering, and symmetry, as illustrated in the example in Figure 3.4

3.3 QA phantoms development

Evaluating heating devices performance, characterizing them, ensuring safety, and assessing long-term stability in terms of QA requires the use of appropriate phantom materials. A phantom is defined as a physical structure assembled using materials that simulate the characteristics of a specific biological tissue as close as practically possible. Especially when considering HT delivered through EM fields, the phantom material has to satisfy particular requirements regarding its properties, together with various practical attributes [107]:

- Good representability of the dielectric properties of the tissues being irradiated for a EM wave propagation that is similar to tissue.
- Thermal properties close to human tissue, both in terms of thermal conductivity and specific heat capacity, to mimic to the best degree possible the distribution of heat in tissue: it is not practical to mimic the effect of blood perfusion, which is a powerful heat sink.

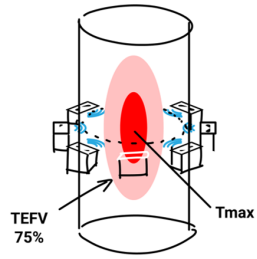

(a) TEFV

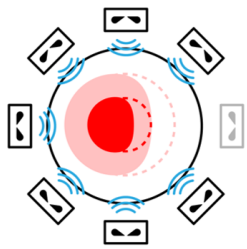

(b) FSym

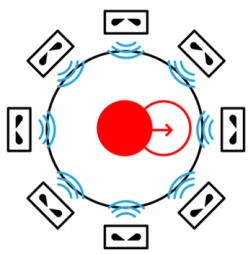

(c) FSteer

Figure 3.3: Graphical representation of the quality parameters used for the applicator characterization according to the new QA protocols for deep HT technology

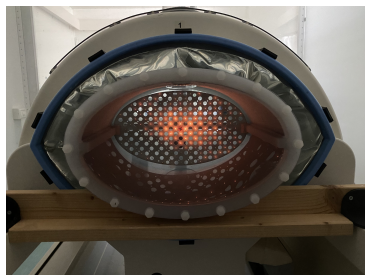

(a) $(x_0, y_0) = (0, 0)$

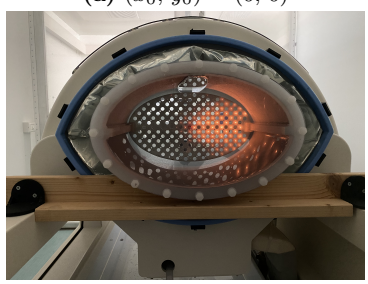

(b) $(x_0, y_0) = (6, 0)$

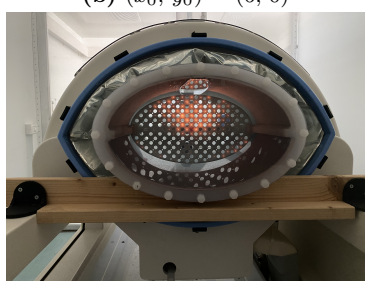

(c) $(x_0, y_0) = (0, 6)$

Figure 3.4: Qualitative evaluation of the steering capability at different locations of the BSD Sigma-Eye applicator (Pyrexar Medical, Salt Lake City, UT, USA) using a custom-built lamp phantom.

- Appropriate mechanical properties, especially at high temperatures. This requirement is essential for solid phantoms, which must maintain their original structure even at elevated temperatures without experiencing structural weakening.
- Stability over time for both dielectric, thermal and mechanical properties
- Easy and reproducible manufacturing protocols
- Use of accessible, inexpensive, and nontoxic materials.

Various phantom materials can be employed for the characterization of HT devices. Phantoms can be broadly categorized into viscous, semi-solid, and solid. Viscous and semi-solid phantoms are primarily utilized to characterize deep HT applicators, while solid phantoms are suitable for deep and superficial HT assessments.

For instance, a well-established semi-solid muscle phantom used extensively for evaluating deep HT devices is based on a mixture of wallpaper paste powder and deionized water [107]. Current popular solid muscle-mimicking models used in the QA of HT devices are sucrose-agar based [114] or the so-called *superstuff* phantom [115]. Formulations for fat-mimicking phantoms are also available. However, these formulations generally suffer from intricate preparation procedures, insufficient thermal or dielectric properties, or limited long-term stability. Examples are a simple solution based on a mixture of flour and oil [116], crystalline nanocellulose reinforcement in gelatin gels [117], and water-free solutions, often referred to as "dry phantoms" [118]–[120].

The following section presents the design of (i) a fat-mimicking phantom consisting of an ethylcellulose-based oleogel and (ii) QA phantoms tailored for deep HT devices.

Ethylcellulose based fat phantom for superficial HT

The availability of an appropriate fat-equivalent phantom represents a challenge for implementing superficial HT QA guidelines: this is especially relevant when considering low-frequency operating devices such as capacitive technology. Fatty tissue has a substantial impact on wave propagation in superficial HT. Several fat-mimicking phantoms have been suggested, but their effectiveness has been constrained by complex fabrication procedures and rapid deterioration challenges. Numerical analysis revealed a significant reduction

of about 40% and 70% for radiative and capacitive HT, respectively, in SAR values in a muscle phantom when adding a top fat layer [71]. These results underline the necessity of a reliable fat-mimicking material to assess superficial HT applicators as accurate as practically possible. Therefore, we propose a new fat-equivalent phantom in Paper A based on an ethylcellulose (EC) gel comprising a glycerol and oil mixture. Due to the EC ability to form oleogels with high melting temperatures, EC-glycerol oleogels are suitable materials to be used routinely in HT QA procedures. Moreover, the absence of water in the fat phantom formulation prevents rapid material degradation and ensures a long shelf life.

Phantom formulation design

Human fatty tissue exhibits different dielectric properties depending on its infiltration level. In the frequency range of 8 MHz to 1 GHz, non-infiltrated fat, due to its lower water content, demonstrates permittivity and conductivity values falling within the intervals of 15 to 5 and 0.03 to 0.05 [S/m], respectively. Conversely, average infiltrated fat displays permittivity values ranging from 32 to 11.3 S/m and conductivity values ranging from 0.05 to 0.11 S/m [121]. Figure 3.5 reports the properties of both average infiltrated and not-infiltrated fat.

Our objective was to adjust the dielectric properties of the phantom to create a material that represents the average properties of fat, falling within the range defined by both infiltrated and non-infiltrated fat. Specifically, we targeted frequencies of 434 MHz and 915 MHz, commonly used for superficial HT treatments. The critical factor to manufacture the phantom with tissue-equivalent properties is the concentration of glycerol in the mixture, which significantly influences the permittivity of the final product and its mechanical stability. As demonstrated by Meney et al. [122], pure glycerol exhibits a permittivity around $\epsilon_r = 40$ for frequencies below 1 GHz, which decreases and stabilizes at $\epsilon_r = 9$ above 1 GHz. Its conductivity displays moderate values, reaching $= 0.5$ S/m for frequencies below 1 GHz. The dielectric properties of glycerol are shown, together with the oil and fat ones, in Figure 3.5. 3.5. Various glycerol concentrations were tested, ranging from 50 wt% to 65 wt% until we identified a concentration of 57 wt%. However, as confirmed by later rheological assessments, the high glycerol concentration negatively impacts the phantom mechanical stability. Therefore, a 57 wt% glycerol concentration

allowed us to achieve the highest possible permittivity without compromising the phantom structural integrity. As reported in [123], an alternative recipe was also developed by decreasing the glycerol concentration to 52 wt% to better address frequencies above 700 MHz.

EC acts as a net-forming agent in the phantom formulation. A crucial parameter for EC is its viscosity, with values between 41 and 49 mPa·s proved effective. Using ethylcellulose with a higher viscosity may compromise the quality of the mixing procedure, leading to air engulfment and complicating phantom handling due to excessively rapid solidification.

The two alternative versions of the recipe, targeting frequencies above and below 700 MHz, respectively, are reported in Table 3.1. The preparation protocol involves three main steps: the creation of a glycerol-in-oil suspension, the addition of EC, and finally, the pouring of the resulting mixture. For the sake of completeness, the entire procedure, described in Paper A, is detailed here:

1. Oil and glycerol are mixed at room temperature. A head-mixer with adjustable speed is used for this purpose (ME SH-11-6C, MESE, Leeds, England). Alternatively, any other suitable device can be used. The mixing speed is adjusted so that no air bubbles are visually present. A mixing speed of 420 rpm was selected for a small batch (∼0.3 kg); 1000 rpm, instead, for a larger batch (∼1.2 kg). Higher mixing speeds would determine excessive trapping of air.

2. Once a visually uniform emulsion is obtained, which takes around 10 min, the temperature is gradually increased to 130°C. A commercially available hot plate is used. The temperature monitoring can be performed by means of a needle-probe thermometer.

3. The EC is then gradually added to the glycerol–oil mix at 130°C until EC is visually dissolved. To ensure thorough dissolution, it is recom-

Table 3.1: concentrations of glycerol, EC, and oil for the fat phantom optimized recipe

Frequency range	Glycerol [wt%]	EC [wt%]	Oil [wt%]
$<$ 700 MHz	57	7	36
$\geq$ 700 MHz	52	8	40

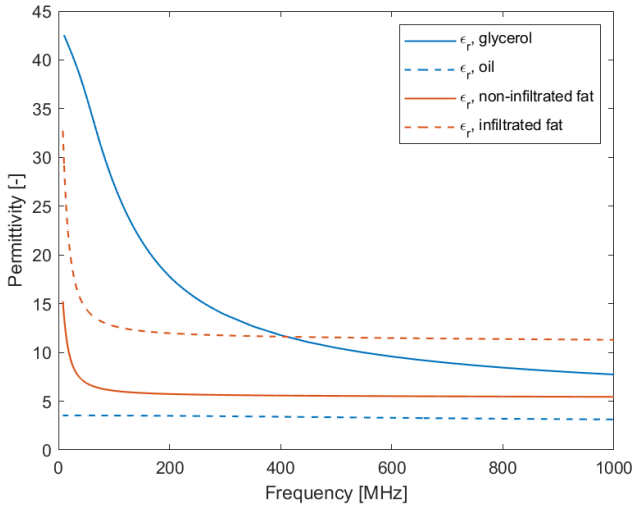

(a)

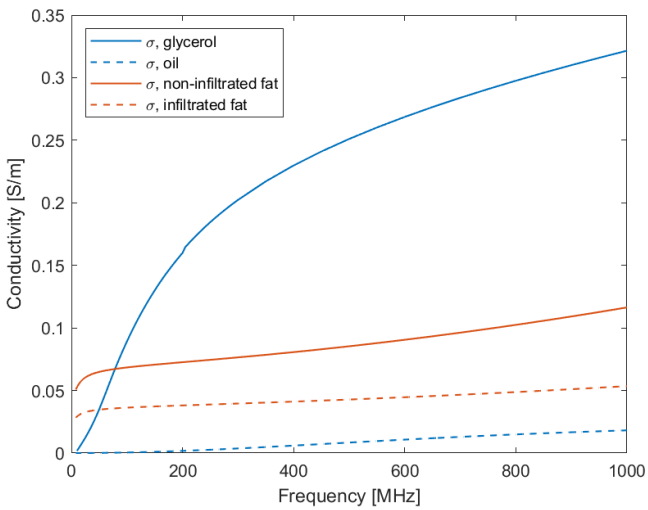

(b)

Figure 3.5: **(a)** Permittivity of average infiltrated fat (orange solid line) and not infiltrated fat (orange dashed line) between 8 MHz and 1 GHz, retrieved from the IT'IS database [121] and permittivity of glycerol (solid blue line) and oil (dashed blue line) measured in the same frequency range; **(b)** Conductivity of fat, oil and glycerol between 8 MHz and 1 GHz. The same color code as **(a)** is used.

mended to use a spoon to break down any larger clumps. It's crucial to confirm that the EC is evenly distributed within the glycerol-oil suspension. Inadequate mixing may result in the EC floating on the surface, potentially leading to the exclusion of part of the glycerol and oil from the final solid gel.

4. The temperature is now increased to 170°C to enable the pouring of the compound into the mold without rapid solidification. During this procedure, the pot should be covered to limit the dispersion of hot vapors.

5. The compound is poured into the desired mold and let to cool down. Using heat-resistant gloves is recommended. It is important to pour the compound quickly: if slowly, the mixture might separate.

6. Once the mixture cools down, the phantom can be stored either in a refrigerator or in a dry environment. Covering the phantom with plastic foil is suggested to avoid bacterial proliferation.

Properties assessment and remarks

Dielectric, thermal, and mechanical properties of the phantom have been characterized according to well-established methodologies, thoroughly described in Paper A. Overall, the phantom presents adequate characteristics, although with limitations in the conductivity at low frequencies. The phantom results in a solid gel, easy to handle, and relatively flexible. Its usability in superficial HT technology assessment has been validated numerically and experimentally (see Paper A). Future work should focus on verifying QA guidelines for superficial capacitive applicators, using this novel fat-mimicking material to experimentally investigate the impact of low conductivity on energy deposition.

Deep HT QA phantoms

To validate phased-array deep HT devices for different tumor locations, it is best to use phantoms specifically tailored to mimic the anatomical characteristics of the region of interest. Following the general recommendations provided by the QA guidelines, a typical QA phantom for deep HT verification comprises an external hard plastic shell (mimicking the external fat layer to some extent) filled with a homogeneous tissue-mimicking material. To assure reproducibility and a low-cost solution, homogeneous phantoms serve

better for QA assessment than heterogeneous anthropomorphic phantoms or elliptical phantoms. The phantom should also be equipped with strategically positioned temperature probes. These probes are strategically placed to capture the temperature distribution within the phantom as accurate as possible, ensuring a robust evaluation of the HT devices performance.

The phantom design process generally focuses on four key parameters:

- Diameter
- Length
- Positioning of the temperature probes
- Tissue mimicking material

The choice of the diameter typically involves a trade-off between the anatomical dimensions of the patient and the physical dimensions of the applicator, all while considering the frequencies used. If the diameter is too small relative to the wavelength, achieving a well-defined focal point can be rendered impractical. In the case of deep HT applicators designed for H&N and limb treatments, which operate within the frequency range of 400-800 MHz, the corresponding wavelength range within muscle-equivalent materials spans from 5 from 10 cm. For the treatment of abdominal and pelvic tumors, where frequencies typically fall between 70 MHz and 120 MHz, the wavelength increases to 30 cm.

For H&N and limb phantoms, the selected diameter should be the average neck diameter in patients affected by H&N malignancies, which is 12 cm [124]: this diameter is compatible with the expected wavelength. For pelvic and abdominal applicators, the selected phantom diameter is 25 cm for devices operating above 75 MHz and 31.5 cm for lower frequencies.

Phantom design

The determination of the phantom length and probe positioning was investigated using electromagnetic-thermal simulations conducted using a multiphysics numerical solver. The impact of catheters and catheter holding structures on the field propagation and heat distribution was also numerically investigated.

The simulation setup should cover several elements to ensure a robust design process, including:

- Using significant frequency points for the treatment area under consideration.
- Employing an applicator model that accurately replicates all EM-relevant characteristics of the actual physical device. This includes the applicator dimensions such as antenna length and shape; number and spacing between antennas; substrate thickness; and electrical properties of any dielectric or materials used in the applicator.
- Using an adequate total input power, considering the dimension of the phantom.
- Incorporating a water bolus with sufficient thickness to prevent excessive reflection to the antenna elements.
- Using a representative material filling, such as a muscle-equivalent gel.

Figure 3.6a illustrates simulation scenarios for the design of a H&N and limb phantom, created using CST MW Studio. In contrast, Figure 3.6b shows the design of a wallpaper paste (WPP) phantom intended for abdominal and pelvic region treatments, generated using COMSOL Multiphysics. In the former case, the applicator comprises ten bow-tie antenna elements [80], [125], while the latter applicator models the BSD Sigma60 device, featuring eight dipole antenna elements.

The simulated SAR and temperature distributions are essential for evaluating the optimal phantom length and determining the probe positioning. Figure 3.7 shows the simulated SAR and the corresponding temperature distribution in a tissue-mimicking phantom with a diameter of 25 cm. An important criterion for assessing the ideal phantom length is the maximum longitudinal extent of the Effective Field Size (EFS), representing the 50% SAR iso distance along the longitudinal axis of the phantom. The optimal phantom length should minimize the presence of standing waves caused by reflections at the phantom edges while avoiding excessive large/heavy phantoms for easy placement of the phantom within the applicator.

Probe positioning was determined by analyzing the SAR and temperature profiles along the X or Y axis on the central X-Y plane of the phantom. The objective is to effectively capture the temperature (or E-field) gradients determined by the applicator, thus defining the location of the focus and the presence of hotspots. Figure 3.8 shows an example of the H&N and limb

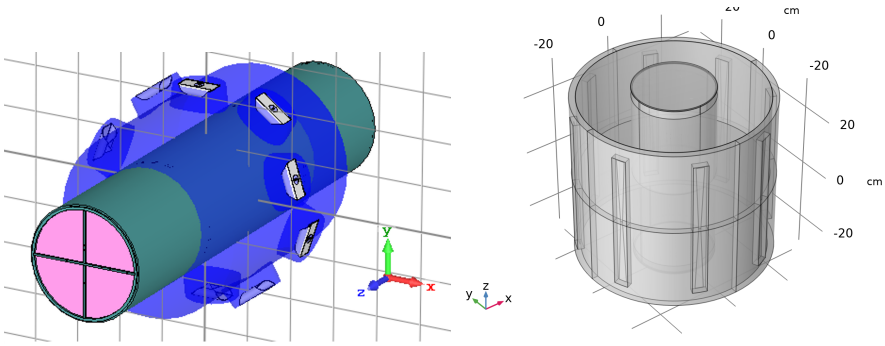

(a) **(b)**

Figure 3.6: Simulation scenarios used for the dimensioning of QA phantoms. Applicator, water bolus and phantom are visible. **(a)** phantom tailored for limb and H&N; **(b)** phantom for abdominal and pelvic region applicators

phantom. The SAR profile reaches its peak at the phantom center and rapidly decays along the x-axis, thus defining the focal area.

The first probe was then positioned at the phantom center (x = 0 cm) to capture the maximum temperature increase. To capture the gradient, we positioned a second and third probes in the middle (1 cm) and end (2 cm) of the focal region. The other two probes were placed at 3 cm and 5 cm from the center to capture the temperature increase in the remaining phantom

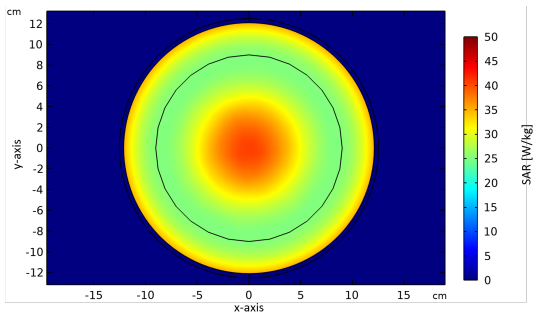

(a)

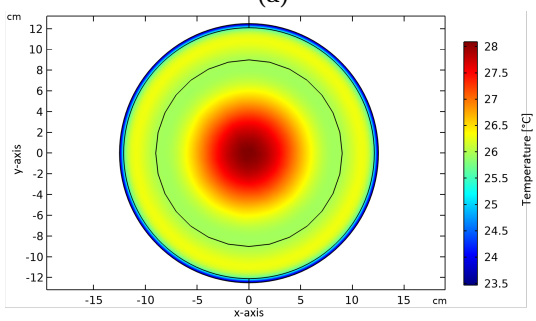

(b)

Figure 3.7: **(a)** simulated SAR on the central plane (z = 0) of a tissue-mimicking phantom with a 25 cm diameter, when a total applied power of 1000 W is applied; **(b)** corresponding temperature distribution after 10 min heating.

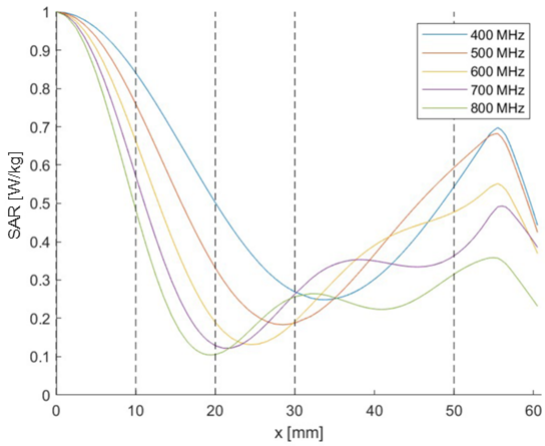

Figure 3.8: Normalized SAR distribution along the x-axis on the phantom central transversal plane at different frequencies. The black dotted lines represent the final position of the measuring probes

CHAPTER 4

Hyperthermia QA protocols: experimental implementation

Translating HT QA guidelines into clinical practice is challenging due to a wide range of uncertainties related to the existing variability of phantom materials and heating and monitoring devices. This chapter focuses on the experimental QA assessment of superficial and deep HT applicators, which allows us to point out the factors affecting the practical implementation of the guidelines. We have adopted the latest QA protocols, which involve the evaluation of quality parameters based on temperature measurements.

4.1 Superficial HT QA assessment

In Paper B [126], we present the QA verification for superficial HT [30] of the lucite cone applicator (LCA) using the most recent ESHO-QA guidelines. The LCA is currently used as a standard device for the treatment of breast cancer recurrences at Erasmus Medical Center, Rotterdam, The Netherlands. This represents the first attempt to assess the LCA using temperature-based metrics. In addition, we created the equivalent computational model of the

device and QA experimental setup to compare with the experimental results.

Experimental procedure

The LCA is shown in Figure 4.1 and consists of a 434 MHz water-filled horn applicator with a square aperture of 10×10 cm^2. Up to six different antenna elements can be combined to treat a total area of 600 cm^2, with independent temperature control for each antenna element.

The LCA QA measurements were performed by evaluating the temperature increase distribution in a layered fat-muscle phantom manufactured following the QA guidelines reported by reference [30]. The phantom consisted of a 1-cm thick phantom layer with fat-mimicking properties overlaying a muscle-mimicking phantom with an overall thickness of 9 cm. The muscle layer was further subdivided into five different layers, as shown in Figure 3.2a. The fat-mimicking layer was produced according to Paper A, while the muscle phantom was based on a superstuff-agar mixture and prepared according to the guidelines [30]. Dielectric and thermal properties of the phantom were verified to be tissue-representative, as explained in paper B.

Six different antenna elements were tested, first each of them independently, then in combinations of two (2×1 array) and four (2×2 array). A similar experimental setup was used for each evaluation. A 434 MHz generator was connected to each LCA antenna through a bidirectional coupler. The forward and reflected power were measured by a power meter through power sensors. The coupling between the antenna(s) and the phantom was provided by a 2-cm thick deionized water bolus, with different lateral dimensions depending on the specific antenna configuration: 20×20 cm^2 for a single antenna, 20×30 cm^2 for the 2×1 array and 45×35 cm^2 for the 2×2 array. Water was circulated in the bolus and antenna horn to maintain a constant temperature. A picture of the experimental setup is shown in Figure 4.1.

In each experiment, the power was turned on for 6 min. Details on transmitted and reflected powers for each antenna configuration can be found in Paper B. During this time frame, a multi-sensor fibreoptic temperature probe assessed the temperature at 1 cm depth in the muscle phantom. The probe was positioned so that its tip corresponded with the center of the antenna aperture. This was done to verify the fulfillment of the temperature rise criteria (6°C in 6 min). After 6 minutes, the antenna(s) and water bolus were removed. The temperature distribution at each layer was assessed using a

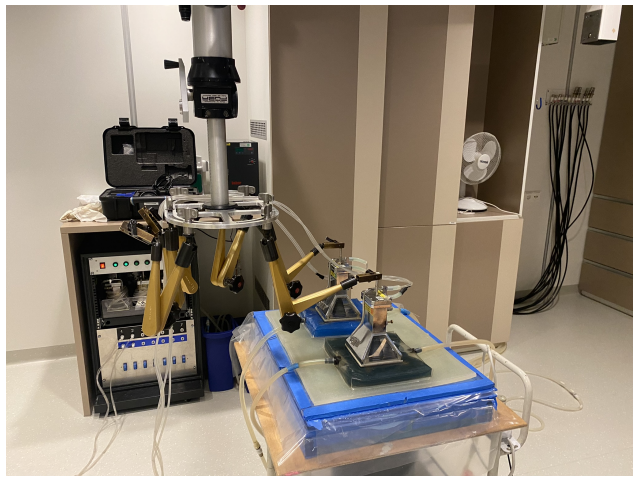

(a)

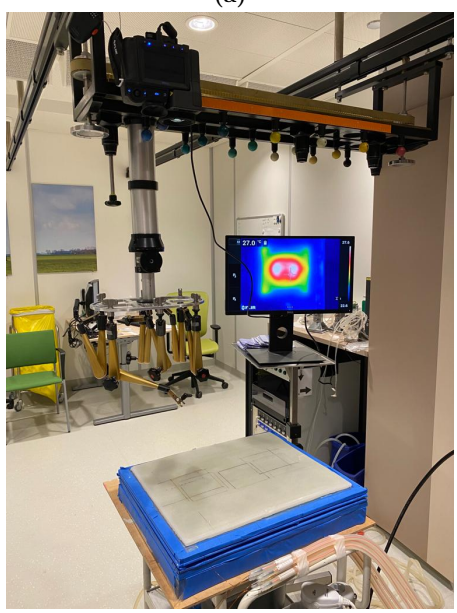

(b)

Figure 4.1: Experimental setup used for the assessment of LCA antennas: (a) LCA antenna elements placed above phantom; (b) temperature distribution captured by the IR camera on the surface of the fat phantom after the removal of the LCA antennas and water bolus.

thermal IR camera mounted perpendicularly over the phantom on a supporting structure. The thermal images were captured with a sequential approach, starting with the measurement of the temperature distribution at 0 cm depth and continuing until reaching the surface at 5.5 cm depth, removing one layer at a time before acquiring a new image. The impact of the heat diffusion during this procedure, which took 60 seconds on average to be completed, was assessed numerically to be irrelevant.

Results of the numerical validation

The heating experiments were recreated through numerical simulations using the Sim4Life software package (v5.2 Zurich MedTech AG, Zurich, Switzerland). Coupled electromagnetic-thermal simulations were conducted, employing a finite-difference time-domain solver. The simulation domain was discretized with a non-uniform grid, which was determined after conducting a mesh independence study. Various total numbers of grid cells were explored to achieve simulations independent of the grid. The temperature increase at 1 cm depth in the fat-muscle phantom was calculated as a function of the number of cells used until a variation less than 5% was found. This resulted in maximum and minimum grid steps of 5 mm and 0.5 mm, respectively.

Energy losses were represented through a combination of Dirichlet and Neumann boundary conditions, serving as inputs for the thermal model. These boundary conditions were applied in correspondence with the phantom – background interface and phantom – water bolus interface. The heat transfer was solved numerically using Pennes' bioheat equation in Sim4Life, with the blood perfusion and metabolic heat terms being zero to exclude terms that are only valid in living tissue. The thermal simulations were scaled to align the input power to the antenna with the net power measured for each antenna during the experiments.

The simulations were run for two distinct phantom models. The first, identified as the "geometrically perfect" model, consisted of a canonical phantom structure with homogeneous layers of fat and muscle materials and having the same dimensions as the manufactured phantom (50 cm $\times$ 40 cm $\times$ 10 cm). The second model was a realistic representation obtained by segmenting a CT scan of the layered phantom used in the experiments. Details on the segmentation procedure can be found in Paper B.

TEFS and TEPD were computed from the simulated temperature distribu-

tions as described in section 3.2. for both phantom models for a quantitative comparison. The best agreement for TEPD was found with the realistic phantom in a multiple antenna configuration. In the case of a single antenna, the two models provided similar results. When assessing the TEFS, the realistic model generally exhibited a closer agreement, although it's worth noting that the canonical model was closer to experimental measurements when using a 2×2 antenna array. Further insights into the results of the comparison between experimental and numerical evaluations can be found in Paper B.

Challenges in the superficial HT guidelines application

The knowledge acquired during the practical application of the superficial HT guidelines and the following comparisons with numerical results offer valuable insights that are here shared to facilitate the translation of QA guidelines into clinical practice. This attempt was the first documented effort to apply the new QA guidelines for superficial HT applications to a radiative device currently in clinical use.

The aim of this research was to reveal the major limitations and challenges while implementing superficial HT guidelines. This is especially relevant considering the expected constraints that can arise from the limited availability of QA equipment in a typical clinical environment:

- **Phantom manufacturing:** The availability of adequate tissue-mimicking supports is essential in the QA assessment of HT devices. The presence of uncertainties in phantom properties and structural inhomogeneities can significantly influence the outcomes of device evaluations: a fact underscored by the comparisons between experimental and simulation results presented in Paper B. To start, the manufacturing process of QA phantoms should be easy to minimize uncertainties while preparing the phantom. In the case of the layered phantom used for the LCA evaluation, producing layers of superstuff-agar muscle phantom presented notable challenges. The high viscosity of the mixture made the entrapment of air inevitable, and achieving uniform layers during casting was difficult. A metal level was used to achieve a more even surface after the mixture was poured into the casting frames. However, this procedure couldn't guarantee the desired precision, leading to unavoidable air pockets between layers. One viable solution is the adoption of another

phantom, such as a sucrose-agar phantom. This material exhibits versatile dielectric properties that can be tailored to specific requirements by adjusting the sucrose-to-salt ratio [114]. Furthermore, the mixture maintains a liquid state right after the preparation, and the solidification process extends over up to 24 hours. As a result, the casting procedure is greatly simplified, as it involves a more straightforward process of simply pouring a liquid mixture into the chosen mold. Another factor to be considered is the relatively short lifetime of these phantoms due to the high water content. The correct storage of the phantoms is essential to avoid excessive evaporation and to prevent mold growth. The use of sucrose-agar phantoms ensures a longer shelf time if correctly stored due to the high sugar concentration.

- **Time constraints:** The entire experimental procedure was over three weeks, including one week to prepare the phantom. We conducted eight distinct experiments comprising six individual antennas and two antenna arrays. A 12-hour gap was maintained between consecutive experiments to allow the phantom to fully equilibrate with room temperature. Additional time was allocated to calibrate the antenna elements to minimize power reflections. Besides the time for the actual experiments, one has to account for the potential to repeat experiments due to execution errors. All factors together resulted in a substantial time commitment, which may be challenging to realize within a clinical setting. However, the QA time commitment at other institutions should be significantly reduced since most use HT devices with single compact applicators, whereas at Erasmus Medical Center they use complex in-house developed antenna arrays. This means the evaluation process could be completed faster, considering the shorter setup times associated with single-antenna applicators

- **Temperature measurement:** The evaluation of temperature distribution is challenging due to many influencing factors, including the temperature of the water bolus and the precise positioning of the applicator. Relying solely on thermal camera measurements may not provide a comprehensive assessment of the temperature distribution generated by the applicator. To reduce uncertainties in temperature assessment, the integration of supplementary temperature probes can be considered.

- **Additional measurements:** The guidelines do not aim to characterize the HT applicators fully, but rather provide the minimum requirements for QA purposes. However, there are experiments that can be executed to provide a comprehensive physical evaluation of the applicator. These include measuring the efficiency of individual antenna elements, exploring phantoms with bone phantoms (or actual large-animal bones), detand ermining the water bolus heat transfer coefficient, among others.

4.2 Deep HT QA assessment

Facilitating device-independent and multi-institutional studies is a primary motivation for developing QA guidelines in HT. While QA procedures have become common, there is still a lack of agreement regarding the protocols to be followed among different institutions. The benefit derived from applying standardized QA protocols is then highly valuable. With this in mind, a comprehensive comparative study was conducted involving six HT centers in Germany and The Netherlands. The primary goal of this study is to evaluate the current performance of hyperthermia devices used for the clinical treatment of deep-seated tumors. The latest version of QA guidelines for deep HT devices is currently being prepared, but the QA procedures have been identified and will be applied in this chapter. The assessment of device performance was carried out in terms of TR and quality metrics, including TEFV, FSteer, and FSym, as described in section 3.2.

Study design

The deep HT QA measurements were conducted using three identical, uniform tissue-mimicking phantoms, as depicted in Figure 4.2. Each phantom features an external cylindrical PVC shell with a thickness of 8 mm and an outer diameter of 25 cm. The phantoms are 60 cm long and were sealed with two waterproof lids. They are equipped with a total of 16 catheters: 14 oriented longitudinally at 3 cm distance from each other, and two are transversely positioned, perpendicular to the longitudinal catheters, intersecting the central plane of the phantom at a 45° angle from each other. Each longitudinal catheter has a length of 30 cm, reaching the central place of the phantom.

The tissue-mimicking phantom gel was manufactured using the ratios: 40

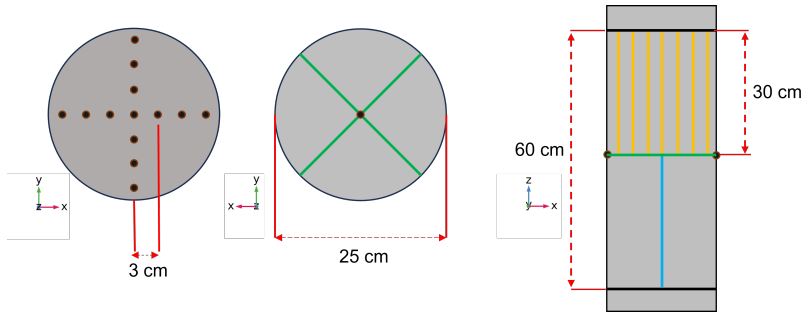

Figure 4.2: Geometry of the phantoms used during the measurement campaign. Left: front X-Y view of the phantom. Each black dot represents the access to one catheter. Middle: back X-Y view. The transversal catheters are represented in green. Right: X-Z view. The longitudinal catheters are represented in yellow.

g/L of perfax wallpaper powder and 3.5 g/L of sodium chloride. Each phantom contains approximately 30 liters of this mixture, prepared in 2-liter batches for easy mixing. The dielectric properties of the resulting solution were assessed in different batches using an open-ended coaxial probe, yielding mean electric permittivity and conductivity values of 65.8 0.5 and 0.63 0.03 S/m, respectively.

The measurements were carried out in the BSD Sigma-60 and BSD Sigma-Eye applicators (Pyrexar Medical, Salt Lake City, USA). For each tested device, six measurements were planned, as outlined in Figure 4.3. The actual number of measurements conducted was 4 on average, mainly due to time and availability constraints. This measurement scheme included three readings with the focal point at the applicator center and three with a steering of 6 cm towards patient top/bottom or left/right.

The temperature increase was assessed using the measurement probes available at each institution. Due to the variability in the number of probes, we set a minimum of three mapping or multi-sensor probes with a total minimum number of sensors of 6. Two of these probes were inserted in the transverse catheters, enabling the analysis of temperature distribution on the central X-Y plane of the phantom, which surrogates the patient axial plane. Another probe was inserted in the longitudinal catheter located in correspondence to the focal point.

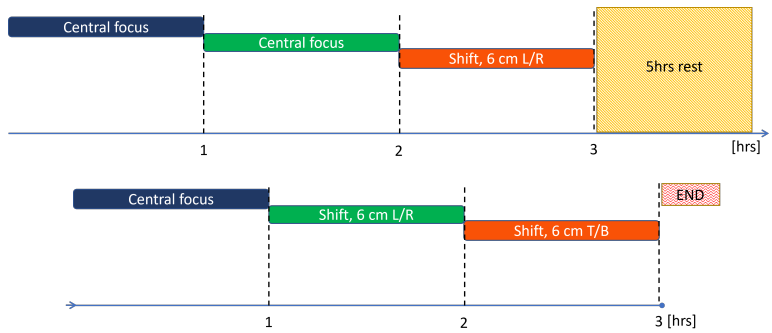

Figure 4.3: Measurement schedule followed for the assessment of a single deep HT device. Each color represents one of the three phantoms. In between two sets of three measurements, a waiting time of 5 h was observed to let each phantom rest for at least 8 h.

When using thermal mapping probes, an initial baseline scan was performed with power off. For multi-sensor probes, the temperature was recorded for few min before proceeding. The power was then turned on for 10 min with a total forward power of 1000 W. At the end of the heating period, a second mapping scan was executed to evaluate the new temperature profile. In cases where a clear focus could not be distinctly identified, a qualitative examination was performed using a lamp phantom.

Following each measurement, an 8-hour interval was observed before reusing the same phantom.

Observations and points of attention

While a comprehensive analysis of quality metrics is still underway, the available data offers valuable insights:

- All the systems met the temperature rise criteria of 6°C within 10 minutes
- Each of the HT devices demonstrated the capability of generating a central focus. The use of a lamp phantom was only required in one institution.

A representative series of temperature measurements is reported in Figure

4.4a. The plot illustrates the temperature profiles recorded by a transversal probe across the central X-Y plane of the phantom for BSD Sigma-60 applicators in four different institutions. The simulated temperature profile is represented with a green dotted curve. A clear peak in temperature rise can be observed around the center of the phantom (12.5 cm along the mapping distance), thus denoting a clearly defined focal spot, with a temperature increase within 10 min between 7.4°C and 9.5°C. The curves recorded in each institution exhibit noticeable discrepancies, which raises concerns that can arise from the institutions and/or from the QA guidelines themselves.

The measured curves for institutions 1 and 4 show the most noticeable offset from the center (in between 2 and 4 cm), while the curves for institutions 2 and 3 generated more symmetrical results. This variance can be attributed to two potential factors:

- External factors occurring during the QA verification: positioning of the phantom within the applicator, the length and quality of thermal sensors, and thermal mapping.

- Malfunctions of the applicator: possible errors in delivered amplitude and phase, water bolus temperature, reflection from the antenna elements.

The phantom was placed manually in the applicator with the assistance of measuring tape or positioning lasers. Custom-made wooden supports were used to ensure the phantom centered positioning within the applicator aperture in the vertical direction. To maintain accurate alignment along the longitudinal axis, efforts were made to keep consistent distances between the applicator edge and the phantom edge on both sides. Additionally, the varying lengths of the temperature probes across institutions contribute to these disparities. While the probes were intended to be fully inserted into the phantom, it is possible that some did not reach the end of the catheters. Furthermore, the precision of thermal mapping must be considered as an additional source of uncertainty. In numerous cases, the thermal mapping process failed to perform correctly, requiring manual intervention, mainly when the probes needed assistance to return to their resting position after the mapping scan. A verification of the thermal mapping through a dry run in a marked catheter can be beneficial, but was not performed for sake of time. An ill-prepared

thermal mapping unit can generate position errors of the order of several cm if the mapping nobs are not tight enough.

Another parameter of influence for the QA results was the presence of hotspots near the phantom walls. This becomes even more pronounced when evaluating the temperature curves normalized to their respective maximum values (as depicted in Figure 4.4b). These observed hotspots could potentially be attributed to applicator performance issues. Possible explanations include: improper calibration of amplitude and phase settings; or cross-coupling between neighboring antenna elements. However, it is worth noting that these hotspots do not manifest when using a lamp phantom. The difference in the power levels used between both experiments – 300 W for the lamp phantom versus 1000 W for the perfax phantom – may play a role, as higher power could potentially induce greater coupling and induced fields between neighboring antenna elements

On the other hand, these hotspots may be attributed to the phantom itself, particularly its permittivity and the increased energy deposition at the plastic-perfax interface. The simulated temperature patterns predicted the presence of near-wall hotspots, but with a much lower amplitude than the ones observed in all experimental sites (Figure 4.4). This outlines that the computational model either needs to be revised or there is some other phenomenon that is not yet being accounted for in the computational model.

Discussion points

Lastly, there are practical insights to be drawn from this measurement campaign:

- Phantom properties: further consideration should be given to the long-term stability of the phantoms, which remains uncertain. The repeated heating and cooling cycles may change the mixture properties, resulting in uncertain outcomes. Thus, weakly measurement of the phantom properties is recommended when possible. Not all users of hyperthermia technology have access to the fabrication and dielectric properties measurement equipment required to perform this studies. A possible solution is for these centers to partner with an academic institution and/or hire dedicated certified companies that provide these services.

- Time constraints: Much like the implementation of superficial guide-

lines, conducting all QA experiments proved to be time-consuming. The manufacturing and filling of the phantom is by itself a lengthy process. Moreover, the temperature measurement process for each applicator required a full day to complete and with the assistance of the entire technical staff.

- Quality parameters evaluation: The presence of hotspots adds complexity to identifying the 75% maximum temperature rise (TR) contour, which is critical to establishing the TEFV as a quality parameter. This complexity arises because the temperature may persist above this threshold due to hotspots. An alternative approach could involve considering a higher threshold, such as the 90% contour, related to the T90 thermal dose measure.

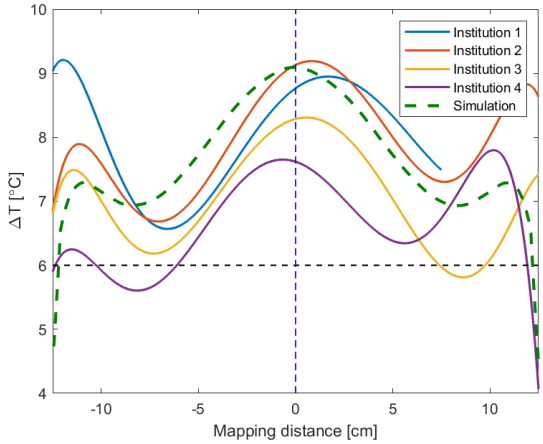

(a) Absolute temperature

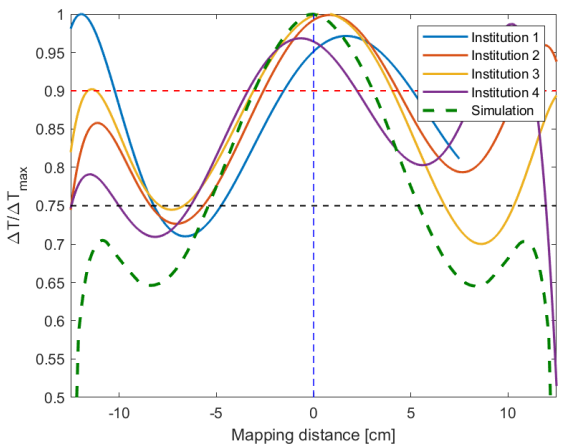

(b) Normalized temperature

Figure 4.4: Experimental temperature measurements in deep HT QA experiments:**(a)** Temperature increase profiles recorded after a 10 min heating period for BSD Sigma-60 applicators in four different institutions using a thermal mapping probe across the X-Y central plane of the phantom. The simulated temperature profile obtained numerically is also reported. The blue vertical dotted line represents the point phantom center; **(b)** normalized temperature increase profiles with respect to the maximum temperature. The simulated normalized temperature profile obtained numerically is also reported. Black and red dotted lines indicate the 75% and 90% isolines.

CHAPTER 5

Summary of included papers

This chapter provides a summary of the included papers.

5.1 Paper A

Mattia De Lazzari, Anna Ström, Laura Farina, Nuno P Silva, Sergio Curto, Hana Dobšíček Trefná
Ethylcellulose-stabilized fat-tissue phantom for quality assurance in clinical hyperthermia
Published in International Journal of Hyperthermia,
vol. 40, no. 1, pp. 2207797, May 2023.
©2023 Taylor & Francis Group, DOI: 10.1080/02656736.2023.2207797 .

This paper introduces an innovative formulation for a fat-mimicking phantom material designed for use in superficial HT QA procedures. This phantom is based on an ethylcellulose (EC) stabilized glycerol-in-oil emulsion. Unlike previous phantom materials, our formulation avoids water, which simplifies the preparation procedure and addresses issues such as inadequate mechanical properties and short shelf life associated with previously proposed phan-

toms. The dielectric, thermal, and rheological properties of the phantom were rigorously assessed through established procedures. Our phantom exhibits representative thermal and mechanical properties, able to withstand high temperatures without weakening its structure. It accurately replicates the dielectric properties of average fat tissue in the frequency range of 200-700 MHz. However, the phantom conductivity falls outside the desired range at lower frequencies (8-200 MHz) and higher frequencies (700 MHz to 1 GHz). Reducing the glycerol concentration to 52 wt% effectively brings the conductivity within the desired range for frequencies above 700 MHz. Unfortunately, no practical solution has been identified to address the low conductivity observed at frequencies below 200 MHz, despite attempts involving the addition of salts like sodium chloride or calcium chloride. Therefore, we illustrate the impact of this reduced conductivity on evaluating capacitive systems using numerical simulations and the standard quality indicators typically used in QA for superficial hyperthermia. Notably, parameters like TEFS and TEPD are overestimated by 13.7% and 23.5%, respectively, due to the phantom low conductivity. This challenge requires further experimental evaluations, particularly concerning capacitive systems. Finally, our phantom underwent testing for compliance with QA guidelines for superficial HT. The experimental results affirm the suitability of our phantom for routine use in superficial HT QA procedures.

5.2 Paper B

Carolina Carrapiço-Seabra, **Mattia De Lazzari**, Abdelali Ameziane, Gerard C van Rhoon, Hana Dobšícek Trefná, Sergio Curto
Application of the ESHO-QA guidelines for determining the performance of the LCA superficial hyperthermia heating system
Published in International Journal of Hyperthermia,
vol. 40, no. 1, pp. 2272578, Oct. 2023.
©2023 Taylor & Francis Group DOI: 10.1080/02656736.2023.2272578 .

This paper evaluates the performance of the Lucite Cone Applicator (LCA) used in superficial HT treatments, assessing their compliance with the latest QA guidelines. Six different antenna elements were examined individually and in combinations of two (2×1 array) and four (2×2 array) antennas. The antennas were tested by measuring the temperature distribution within a fat-

muscle layered phantom prepared following the guideline recommendations. The obtained temperature distributions were used to assess whether the Temperature Rise (TR) criteria were met and to evaluate two essential quality metrics: Thermal Effective Field Size (TEFS) and Thermal Effective Depth (TEPD). The results indicated that all LCAs satisfied the TR criteria, causing a maximum temperature increase greater than 6°C at a depth of 2 cm in the fat-muscle phantom. We also compared the experimental results with simulations conducted using a standard phantom model and a realistic model segmented from CT imaging data. The mean negative difference between simulated and experimental data was 1.3°C when employing the standard phantom model, which was reduced to a mean negative difference of 0.4°C when using the realistic model. Simulated and measured TEPD exhibited good agreement for both scenarios, while some disparities were observed for TEFS. The paper highlights various uncertainties during QA procedures, such as antenna positioning, applicator efficiency, water bolus utilization, and heat transfer coefficients. It suggests that further characterization of these parameters can improve the accuracy of QA assessments. Lastly, the paper puts into evidence the time-consuming and demanding nature of implementing QA guidelines, especially in preparing uniform phantoms and ensuring the proper setup of antenna elements, emphasizing the need for meticulous phantom preparation and experimental setup for reliable QA results.

CHAPTER 6

Concluding Remarks and Future Work

This thesis focuses on the practical implementation of the most recent QA guidelines in clinical HT, while providing new solutions to make these guidelines more practical and relevant to hyperthermia applications. To this end, both deep and superficial HT applicators were thoroughly investigated for the first time using most up to date QA protocols. This research will highlight practical aspects and identify potential limitations associated with the underexplored HT QA process, which is critical for a successful HT treatment delivery.

A critical prerequisite for successfully implementing QA guidelines is the availability of appropriate tissue-mimicking materials with physical properties as close to human tissues as possible. For deep HT, the gel phantom proposed in QA guidelines was easy to manufacture and handle, but the superficial HT phantom lacked the critical superficial fat layer that is present in the human body. Consequently, we proposed a novel ethylcellulose-based fat-mimicking phantom for the QA assessment of superficial HT devices.

The results from the fat-phantom demonstrate its suitability for verifying the HT performance of radiative superficial HT applicators. The material exhibits satisfactory thermal, mechanical, and dielectric properties within the

related frequency range. However, significant limitations arise when applying this phantom to verify capacitive devices, primarily due to the low conductivity of the material. Future work should focus on conducting thorough experimental verifications using this material for capacitive devices. This will allow us to understand the impact of low conductivity on energy deposition. Additionally, efforts are underway to refine the phantom formulation by incorporating salts to enhance conductivity.

General considerations apply to both deep and superficial QA protocols. Common challenges in implementing guidelines include the properties of phantom materials, time constraints, and availability of suitable equipment. Inhomogeneities in the phantom structure and properties significantly impact the final QA evaluation, especially when compared to simulated data (as shown in paper B). Manufacturing the phantom for superficial QA verification also proved challenging in achieving gel homogeneity. Hence, exploring alternative phantom formulations may be worth considering. This underscores the need for straightforward phantom preparation protocols. Moreover, ensuring the stability of phantom properties over time is critical, mainly when the phantom material is intended for potential long-term use. A periodic verification of the phantom properties should be considered as an additional step to the QA evaluation.

The availability of suitable measurement equipment is essential and should be verified before conducting QA evaluations. In the evaluation of deep HT devices, we identified that a minimum of three mapping or multi-sensor probes is required to ensure a proper assessment of the QA indicators outlined in the guidelines. Preliminary verification prior to the QA assessment involves proper calibration and confirmation of the functionality of temperature probes, including a thorough check of the thermal mapping mechanism.

Regarding the QA evaluation for deep HT, the analysis of results is currently underway and is expected to provide more insights into the current performance of deep HT devices. The results to date indicate that all devices met the minimum temperature increase requirement. However, there are two phenomena that remain unclear due to either device performance or measurement procedures: hotspots observed near the phantom wall and central focus asymmetries. are linked.

Future work involves evaluating deep HT devices operating at lower frequencies, such as at 70 MHz. The challenge here lies in achieving a distinct

focal spot in the phantom center while minimizing superficial hotspots.

Another prospective step is a systematic and experimental comparison between QA evaluations of deep HT devices based on SAR and temperature. While the theoretical parallelism between the two is evident, an experimental assessment could be beneficial. This approach may aid in understanding the observed differences between lamp phantom measurements and tissue-mimicking ones.

References

[1] J. Ferlay, M. Ervik, F. Lam, *et al.*, "Observatory:"cancer today". lyon international agency res," *Cancer*, 2020.

[2] WHO, *Cancer*, Feb. 2022.

[3] K. D. Miller, L. Nogueira, T. Devasia, *et al.*, "Cancer treatment and survivorship statistics, 2022," *CA: a cancer journal for clinicians*, vol. 72, no. 5, pp. 409–436, 2022.

[4] D. T. Debela, S. G. Muzazu, K. D. Heraro, *et al.*, "New approaches and procedures for cancer treatment: Current perspectives," *SAGE open medicine*, vol. 9, p. 20 503 121 211 034 366, 2021.

[5] M. Horsman and J. Overgaard, "Hyperthermia: A potent enhancer of radiotherapy," *Clinical oncology*, vol. 19, no. 6, pp. 418–426, 2007.

[6] R. D. Issels, "Hyperthermia adds to chemotherapy," *European journal of cancer*, vol. 44, no. 17, pp. 2546–2554, 2008.

[7] C. Vernon, J. Hand, S. Field, D. Machin, and J. Whaley, "Van der zj, van putten wl, van rhoon gc, van dijk jd, gonzalez gd, et al. radiotherapy with or without hyperthermia in the treatment of superficial localized breast cancer: Results from five randomized controlled trials. international collaborative hyperthermia group," *Int J Radiat Oncol Biol Phys*, vol. 35, pp. 731–744, 1996.

[8] R. D. Issels, L. H. Lindner, J. Verweij, *et al.*, "Neo-adjuvant chemotherapy alone or with regional hyperthermia for localised high-risk soft-tissue sarcoma: A randomised phase 3 multicentre study," *The lancet oncology*, vol. 11, no. 6, pp. 561–570, 2010.

[9] R. D. Issels, L. H. Lindner, J. Verweij, *et al.*, "Effect of neoadjuvant chemotherapy plus regional hyperthermia on long-term outcomes among patients with localized high-risk soft tissue sarcoma: The eortc 62961-esho 95 randomized clinical trial," *JAMA oncology*, vol. 4, no. 4, pp. 483–492, 2018.

[10] J. van der Zee, D. González, G. C. van Rhoon, J. D. van Dijk, W. L. van Putten, and A. A. Hart, "Comparison of radiotherapy alone with radiotherapy plus hyperthermia in locally advanced pelvic tumours: A prospective, randomised, multicentre trial," *The Lancet*, vol. 355, no. 9210, pp. 1119–1125, 2000.

[11] Y. Harima, T. Ohguri, H. Imada, *et al.*, "A multicentre randomised clinical trial of chemoradiotherapy plus hyperthermia versus chemoradiotherapy alone in patients with locally advanced cervical cancer," *International journal of hyperthermia*, vol. 32, no. 7, pp. 801–808, 2016.

[12] R. Issels, L. Lindner, P. Wust, *et al.*, "Regional hyperthermia (rht) improves response and survival when combined with systemic chemotherapy in the management of locally advanced, high grade soft tissue sarcomas (sts) of the extremities, the body wall and the abdomen: A phase iii randomised pros," *Journal of Clinical Oncology*, vol. 25, no. 18_suppl, pp. 10 009–10 009, 2007.

[13] E. L. Jones, T. V. Samulski, M. W. Dewhirst, *et al.*, "A pilot phase ii trial of concurrent radiotherapy, chemotherapy, and hyperthermia for locally advanced cervical carcinoma," *Cancer*, vol. 98, no. 2, pp. 277–282, 2003.

[14] N. R. Datta, E. Puric, D. Klingbiel, S. Gomez, and S. Bodis, "Hyperthermia and radiation therapy in locoregional recurrent breast cancers: A systematic review and meta-analysis," *International Journal of Radiation Oncology* Biology* Physics*, vol. 94, no. 5, pp. 1073–1087, 2016.

[15] D. F. De Haas-Kock, J. Buijsen, M. Pijls-Johannesma, *et al.*, "Concomitant hyperthermia and radiation therapy for treating locally advanced rectal cancer," *Cochrane Database of Systematic Reviews*, no. 3, 2009.

[16] A. Vasanthan, M. Mitsumori, J. H. Park, *et al.*, "Regional hyperthermia combined with radiotherapy for uterine cervical cancers: A multi-institutional prospective randomized trial of the international atomic energy agency," *International Journal of Radiation Oncology* Biology* Physics*, vol. 61, no. 1, pp. 145–153, 2005.

[17] N. R. Datta, E. Stutz, S. Gomez, and S. Bodis, "Efficacy and safety evaluation of the various therapeutic options in locally advanced cervix cancer: A systematic review and network meta-analysis of randomized clinical trials," *International Journal of Radiation Oncology* Biology* Physics*, vol. 103, no. 2, pp. 411–437, 2019.

[18] P. W. Chiu, A. C. Chan, S. Leung, *et al.*, "Multicenter prospective randomized trial comparing standard esophagectomy with chemoradiotherapy for treatment of squamous esophageal cancer: Early results from the chinese university research group for esophageal cancer (cure)," *Journal of gastrointestinal surgery*, vol. 9, pp. 794–802, 2005.

[19] N. R. Datta, S. Rogers, S. G. Ordóñez, E. Puric, and S. Bodis, "Hyperthermia and radiotherapy in the management of head and neck cancers: A systematic review and meta-analysis," *International Journal of Hyperthermia*, vol. 32, no. 1, pp. 31–40, 2016.

[20] P. D. Veltsista, E. Oberacker, A. Ademaj, *et al.*, "Hyperthermia in the treatment of high-risk soft tissue sarcomas: A systematic review," *International Journal of Hyperthermia*, vol. 40, no. 1, p. 2 236 337, 2023.

[21] J. Overgaard, S. Bentzen, D. G. Gonzalez, *et al.*, "Randomised trial of hyperthermia as adjuvant to radiotherapy for recurrent or metastatic malignant melanoma," *The Lancet*, vol. 345, no. 8949, pp. 540–543, 1995.

[22] C. A. Perez, B. Gillespie, T. Pajak, N. B. Hornback, D. Emami, and P. Rubin, "Quality assurance problems in clinical hyperthermia and their impact on therapeutic outcome: A report by the radiation therapy oncology group," *International Journal of Radiation Oncology* Biology* Physics*, vol. 16, no. 3, pp. 551–558, 1989.

[23] J. R. Oleson, T. V. Samulski, K. A. Leopold, *et al.*, "Sensitivity of hyperthermia trial outcomes to temperature and time: Implications for thermal goals of treatment," *International Journal of Radiation Oncology* Biology* Physics*, vol. 25, no. 2, pp. 289–297, 1993.

[24] M. Sherar, F.-F. Liu, M. Pintilie, *et al.*, "Relationship between thermal dose and outcome in thermoradiotherapy treatments for superficial recurrences of breast cancer: Data from a phase iii trial," *International Journal of Radiation Oncology* Biology* Physics*, vol. 39, no. 2, pp. 371–380, 1997.

[25] A. Bakker, J. van der Zee, G. van Tienhoven, H. P. Kok, C. R. Rasch, and H. Crezee, "Temperature and thermal dose during radiotherapy and hyperthermia for recurrent breast cancer are related to clinical outcome and thermal toxicity: A systematic review," *International Journal of Hyperthermia*, vol. 36, no. 1, pp. 1023–1038, 2019.

[26] E. L. Jones, J. R. Oleson, L. R. Prosnitz, *et al.*, "Randomized trial of hyperthermia and radiation for superficial tumors," *Journal of clinical oncology*, vol. 23, no. 13, pp. 3079–3085, 2005.

[27] M. Franckena, D. Fatehi, M. de Bruijne, *et al.*, "Hyperthermia dose-effect relationship in 420 patients with cervical cancer treated with combined radiotherapy and hyperthermia," *European Journal of Cancer*, vol. 45, no. 11, pp. 1969–1978, 2009.

[28] M. Kroesen, H. T. Mulder, J. M. van Holthe, *et al.*, "Confirmation of thermal dose as a predictor of local control in cervical carcinoma patients treated with state-of-the-art radiation therapy and hyperthermia," *Radiotherapy and oncology*, vol. 140, pp. 150–158, 2019.

[29] H. D. Trefná, H. Crezee, M. Schmidt, *et al.*, "Quality assurance guidelines for superficial hyperthermia clinical trials: I. clinical requirements," *International Journal of Hyperthermia*, vol. 33, no. 4, pp. 471–482, 2017.

[30] H. Dobšiček Trefná, J. Crezee, M. Schmidt, *et al.*, "Quality assurance guidelines for superficial hyperthermia clinical trials: Ii. technical requirements for heating devices," *Strahlentherapie und Onkologie*, vol. 193, no. 5, pp. 351–366, 2017.

[31] H. Dobšiček Trefná, M. Schmidt, G. Van Rhoon, *et al.*, "Quality assurance guidelines for interstitial hyperthermia," *International Journal of Hyperthermia*, vol. 36, no. 1, pp. 276–293, 2019.

[32] G. Bruggmoser, S. Bauchowitz, R. Canters, *et al.*, "Guideline for the clinical application, documentation and analysis of clinical studies for regional deep hyperthermia," *Strahlenther. Onkol*, vol. 188, pp. 198–211, 2012.

[33] G. Bruggmoser, S. Bauchowitz, R. Canters, *et al.*, "Quality assurance for clinical studies in regional deep hyperthermia," *Strahlentherapie und Onkologie*, vol. 187, no. 10, p. 605, 2011.

[34] I. C. on Non-Ionizing Radiation Protection *et al.*, "Principles for non-ionizing radiation protection," *Health physics*, vol. 118, no. 5, pp. 477–482, 2020.

[35] O. Desouky, N. Ding, and G. Zhou, "Targeted and non-targeted effects of ionizing radiation," *Journal of Radiation Research and Applied Sciences*, vol. 8, no. 2, pp. 247–254, 2015.

[36] G. Borrego-Soto, R. Ortiz-López, and A. Rojas-Martınez, "Ionizing radiation-induced dna injury and damage detection in patients with breast cancer," *Genetics and molecular biology*, vol. 38, pp. 420–432, 2015.

[37] J. Stauffer and M. Paulides, "Hyperthermia therapy for cancer," 2014.

[38] E. H. Wissler, "Pennes' 1948 paper revisited," *Journal of applied physiology*, vol. 85, no. 1, pp. 35–41, 1998.

[39] G. Delaney, S. Jacob, C. Featherstone, and M. Barton, "The role of radiotherapy in cancer treatment: Estimating optimal utilization from a review of evidence-based clinical guidelines," *Cancer: Interdisciplinary International Journal of the American Cancer Society*, vol. 104, no. 6, pp. 1129–1137, 2005.

[40] P. R. Stauffer, "Evolving technology for thermal therapy of cancer," *International Journal of Hyperthermia*, vol. 21, no. 8, pp. 731–744, 2005.

[41] K. F. Chu and D. E. Dupuy, "Thermal ablation of tumours: Biological mechanisms and advances in therapy," *Nature Reviews Cancer*, vol. 14, no. 3, pp. 199–208, 2014.

[42] M. Ahmed, L. Solbiati, C. L. Brace, *et al.*, "Image-guided tumor ablation: Standardization of terminology and reporting criteria—a 10-year update," *Radiology*, vol. 273, no. 1, pp. 241–260, 2014.

[43] S. N. Goldberg, G. S. Gazelle, and P. R. Mueller, "Thermal ablation therapy for focal malignancy: A unified approach to underlying principles, techniques, and diagnostic imaging guidance," *American journal of roentgenology*, vol. 174, no. 2, pp. 323–331, 2000.

[44] P. Prakash, "Theoretical modeling for hepatic microwave ablation," *The open biomedical engineering journal*, vol. 4, p. 27, 2010.

[45] Z. Vujaskovic and C. Song, "Physiological mechanisms underlying heat-induced radiosensitization," *International Journal of Hyperthermia*, vol. 20, no. 2, pp. 163–174, 2004.

[46] W. Dewey, "Interaction of heat with radiation and chemotherapy," *Cancer research*, vol. 44, no. 10_Supplement, 4714s–4720s, 1984.

[47] N. van den Tempel, M. R. Horsman, and R. Kanaar, "Improving efficacy of hyperthermia in oncology by exploiting biological mechanisms," *International journal of hyperthermia*, vol. 32, no. 4, pp. 446–454, 2016.

[48] A. Oei, H. Kok, S. Oei, *et al.*, "Molecular and biological rationale of hyperthermia as radio-and chemosensitizer," *Advanced drug delivery reviews*, vol. 163, pp. 84–97, 2020.

[49] S. Field and C. Morris, "The relationship between heating time and temperature: Its relevance to clinical hyperthermia," *Radiotherapy and Oncology*, vol. 1, no. 2, pp. 179–186, 1983.

[50] X. Sun, L. Xing, C. Clifton Ling, and G. C. Li, "The effect of mild temperature hyperthermia on tumour hypoxia and blood perfusion: Relevance for radiotherapy, vascular targeting and imaging," *International Journal of Hyperthermia*, vol. 26, no. 3, pp. 224–231, 2010.

[51] M. B. Lande, J. M. Donovan, and M. L. Zeidel, "The relationship between membrane fluidity and permeabilities to water, solutes, ammonia, and protons.," *The Journal of general physiology*, vol. 106, no. 1, pp. 67–84, 1995.

[52] S. Toraya-Brown and S. Fiering, "Local tumour hyperthermia as immunotherapy for metastatic cancer," *International journal of hyperthermia*, vol. 30, no. 8, pp. 531–539, 2014.

[53] J. M. Bull, "A review of immune therapy in cancer and a question: Can thermal therapy increase tumor response?" *International Journal of Hyperthermia*, vol. 34, no. 6, pp. 840–852, 2018.

[54] S. S. Evans, E. A. Repasky, and D. T. Fisher, "Fever and the thermal regulation of immunity: The immune system feels the heat," *Nature Reviews Immunology*, vol. 15, no. 6, pp. 335–349, 2015.

[55] A. L. Oei, L. E. Vriend, J. Crezee, N. A. Franken, and P. M. Krawczyk, "Effects of hyperthermia on dna repair pathways: One treatment to inhibit them all," *Radiation Oncology*, vol. 10, pp. 1–13, 2015.

[56] M. Jasin and R. Rothstein, "Repair of strand breaks by homologous recombination," *Cold Spring Harbor perspectives in biology*, vol. 5, no. 11, a012740, 2013.

[57] N. van den Tempel, C. Laffeber, H. Odijk, *et al.*, "The effect of thermal dose on hyperthermia-mediated inhibition of dna repair through homologous recombination," *Oncotarget*, vol. 8, no. 27, p. 44 593, 2017.

[58] J. Lepock, "Role of nuclear protein denaturation and aggregation in thermal radiosensitization," *International journal of hyperthermia*, vol. 20, no. 2, pp. 115–130, 2004.

[59] S. A. Sapareto and W. C. Dewey, "Thermal dose determination in cancer therapy," *International Journal of Radiation Oncology* Biology* Physics*, vol. 10, no. 6, pp. 787–800, 1984.

[60] M. W. Dewhirst, B. Viglianti, M. Lora-Michiels, M. Hanson, and P. Hoopes, "Basic principles of thermal dosimetry and thermal thresholds for tissue damage from hyperthermia," *International journal of hyperthermia*, vol. 19, no. 3, pp. 267–294, 2003.

[61] W. C. Dewey and C. J. Diederich, "Hyperthermia classic commentary:'arrhenius relationships from the molecule and cell to the clinic'by william dewey, int. j. hyperthermia, 10: 457–483, 1994," *International journal of hyperthermia*, vol. 25, no. 1, pp. 21–24, 2009.

[62] G. C. van Rhoon, "Is cem43 still a relevant thermal dose parameter for hyperthermia treatment monitoring?" *International Journal of Hyperthermia*, vol. 32, no. 1, pp. 50–62, 2016.

[63] G. Schooneveldt, A. Bakker, E. Balidemaj, *et al.*, "Thermal dosimetry for bladder hyperthermia treatment. an overview," *International Journal of Hyperthermia*, vol. 32, no. 4, pp. 417–433, 2016.

[64] N. R. Datta, D. Marder, S. Datta, *et al.*, "Quantification of thermal dose in moderate clinical hyperthermia with radiotherapy: A relook using temperature–time area under the curve (auc)," *International journal of hyperthermia*, vol. 38, no. 1, pp. 296–307, 2021.

[65] C. Carrapiço-Seabra, S. Curto, M. Franckena, and G. C. V. Rhoon, "Avoiding pitfalls in thermal dose effect relationship studies: A review and guide forward," *Cancers*, vol. 14, no. 19, p. 4795, 2022.

[66] H. P. Kok, E. N. Cressman, W. Ceelen, *et al.*, "Heating technology for malignant tumors: A review," *International Journal of Hyperthermia*, vol. 37, no. 1, pp. 711–741, 2020.

[67] M. Paulides, H. D. Trefna, S. Curto, and D. Rodrigues, "Recent technological advancements in radiofrequency-andmicrowave-mediated hyperthermia for enhancing drug delivery," *Advanced drug delivery reviews*, vol. 163, pp. 3–18, 2020.

[68] G. Van Rhoon, P. Rietveld, and J. Van der Zee, "A 433 mhz lucite cone waveguide applicator for superficial hyperthermia," *International journal of hyperthermia*, vol. 14, no. 1, pp. 13–27, 1998.

[69] P. R. Stauffer, P. Maccarini, K. Arunachalam, *et al.*, "Conformal microwave array (cma) applicators for hyperthermia of diffuse chest wall recurrence," *International Journal of Hyperthermia*, vol. 26, no. 7, pp. 686–698, 2010.

[70] H. Kok, F. Navarro, L. Strigari, M. Cavagnaro, and J. Crezee, "Locoregional hyperthermia of deep-seated tumours applied with capacitive and radiative systems: A simulation study," *International Journal of Hyperthermia*, vol. 34, no. 6, pp. 714–730, 2018.

[71] H. Kok and J. Crezee, "A comparison of the heating characteristics of capacitive and radiative superficial hyperthermia," *International Journal of Hyperthermia*, vol. 33, no. 4, pp. 378–386, 2017.

[72] M. Hiraoka, S. Jo, K. Akuta, Y. Nishimura, M. Takahashi, and M. Abe, "Radiofrequency capacitive hyperthermia for deep-seated tumors. i. studies on thermometry," *Cancer*, vol. 60, no. 1, pp. 121–127, 1987.

[73] M. Notter, H. Piazena, and P. Vaupel, "Hypofractionated re-irradiation of large-sized recurrent breast cancer with thermography-controlled, contact-free water-filtered infra-red-a hyperthermia: A retrospective study of 73 patients," *International Journal of Hyperthermia*, vol. 33, no. 2, pp. 227–236, 2017.

[74] J. v. d. Zee and D. G. González, "The dutch deep hyperthermia trial: Results in cervical cancer," *International journal of hyperthermia*, vol. 18, no. 1, pp. 1–12, 2002.

[75] O. J. Ott, U. S. Gaipl, A. Lamrani, and R. Fietkau, "The emerging evidence supporting integration of deep regional hyperthermia with chemoradiation in bladder cancer," in *Seminars in Radiation Oncology*, Elsevier, vol. 33, 2023, pp. 82–90.

[76] R. Wessalowski, D. T. Schneider, O. Mils, *et al.*, "Regional deep hyperthermia for salvage treatment of children and adolescents with refractory or recurrent non-testicular malignant germ-cell tumours: An open-label, non-randomised, single-institution, phase 2 study," *The lancet oncology*, vol. 14, no. 9, pp. 843–852, 2013.

[77] H. Kok, M. De Greef, P. Borsboom, A. Bel, and J. Crezee, "Improved power steering with double and triple ring waveguide systems: The impact of the operating frequency," *International Journal of Hyperthermia*, vol. 27, no. 3, pp. 224–239, 2011.

[78] D. P. KEITH, S. GEIMER, T. JINGWU, and E. B. WILLIAM, "Optimization of pelvic heating rate distributions with electromagnetic phased arrays," *International journal of hyperthermia*, vol. 15, no. 3, pp. 157–186, 1999.

[79] M. Paulides, Z. Rijnen, P. Togni, *et al.*, "Clinical introduction of novel microwave hyperthermia technology: The hypercollar3d applicator for head and neck hyperthermia," in *2015 9th European Conference on Antennas and Propagation (EuCAP)*, IEEE, 2015, pp. 1–4.

[80] P. Takook, M. Shafiemehr, M. Persson, and H. D. Trefná, "Experimental evaluation of uwb applicator prototype for head and neck hyperthermia," in *2017 11th European Conference on Antennas and Propagation (EUCAP)*, IEEE, 2017, pp. 3619–3620.

[81] T. P. Ryan and C. L. Brace, "Interstitial microwave treatment for cancer: Historical basis and current techniques in antenna design and performance," *International Journal of Hyperthermia*, vol. 33, no. 1, pp. 3–14, 2017.

[82] P. K. Sneed, P. R. Stauffer, M. W. McDermott, *et al.*, "Survival benefit of hyperthermia in a prospective randomized trial of brachytherapy boost±hyperthermia for glioblastoma multiforme," *International Journal of Radiation Oncology* Biology* Physics*, vol. 40, no. 2, pp. 287–295, 1998.

[83] C. Coughlin, E. Douple, J. Strohbehn, W. Eaton Jr, B. Trembly, and T. Wong, "Interstitial hyperthermia in combination with brachytherapy.," *Radiology*, vol. 148, no. 1, pp. 285–288, 1983.

[84] G. Lassche, J. Crezee, and C. Van Herpen, "Whole-body hyperthermia in combination with systemic therapy in advanced solid malignancies," *Critical reviews in oncology/hematology*, vol. 139, pp. 67–74, 2019.

[85] J. M. Bull, G. L. Scott, F. R. Strebel, *et al.*, "Fever-range whole-body thermal therapy combined with cisplatin, gemcitabine, and daily interferon-α: A description of a phase i-ii protocol," *International Journal of Hyperthermia*, vol. 24, no. 8, pp. 649–662, 2008.

[86] J. Shafiq, M. Barton, D. Noble, C. Lemer, and L. J. Donaldson, "An international review of patient safety measures in radiotherapy practice," *Radiotherapy and Oncology*, vol. 92, no. 1, pp. 15–21, 2009.

[87] Y. Chen, J. Williams, I. Ding, *et al.*, "Radiation pneumonitis and early circulatory cytokine markers," in *Seminars in radiation oncology*, Elsevier, vol. 12, 2002, pp. 26–33.

[88] H. Majeed and V. Gupta, "Adverse effects of radiation therapy," 2020.

[89] H. Omer, "Radiobiological effects and medical applications of non-ionizing radiation," *Saudi journal of biological sciences*, vol. 28, no. 10, pp. 5585–5592, 2021.

[90] J. A. D'Andrea, J. M. Ziriax, and E. R. Adair, "Radio frequency electromagnetic fields: Mild hyperthermia and safety standards," *Progress in brain research*, vol. 162, pp. 107–135, 2007.

[91] W. H. Bailey, R. Bodemann, J. Bushberg, *et al.*, "Synopsis of ieee std c95. 1™-2019 "ieee standard for safety levels with respect to human exposure to electric, magnetic, and electromagnetic fields, 0 hz to 300 ghz"," *IEEE Access*, vol. 7, pp. 171 346–171 356, 2019.

[92] I. C. on Non-Ionizing Radiation Protection *et al.*, "Guidelines for limiting exposure to electromagnetic fields (100 khz to 300 ghz)," *Health physics*, vol. 118, no. 5, pp. 483–524, 2020.

[93] "Quality management systems — Fundamentals and vocabulary," International Organization for Standardization, Geneva, CH, Standard, 2015.

[94] C. B. Saw, M. S. Ferenci, and H. Wanger Jr, "Technical aspects of quality assurance in radiation oncology," *Biomedical imaging and intervention journal*, vol. 4, no. 3, 2008.

[95] J. Hand, J. Lagenduk, J. B. Andersen, and J. C. Bolomey, "Quality assurance guidelines for esho protocols," *International Journal of Hyperthermia*, vol. 5, no. 4, pp. 421–428, 1989.

[96] J. Lagendijk, G. Van Rhoon, S. Hornsleth, *et al.*, "Esho quality assurance guidelines for regional hyperthermia," *International journal of hyperthermia*, vol. 14, no. 2, pp. 125–133, 1998.

[97] M. Dewhirst, T. Phillips, T. Samulski, *et al.*, "Rtog quality assurance guidelines for clinical trials using hyperthermia," *International Journal of Radiation Oncology* Biology* Physics*, vol. 18, no. 5, pp. 1249–1259, 1990.

[98] D. I. Thwaites, B. Mijnheer, and J. A. Mills, "Quality assurance of external beam radiotherapy," *Radiation oncology physics: a handbook for teachers and students. Vienna: International Atomic Energy Agency*, pp. 407–450, 2005.

[99] R. J. Shalek, "Determination of absorbed dose in a patient irradiated by beams of x or gamma rays in radiotherapy procedures," *Medical Physics*, vol. 4, no. 5, p. 461, 1977.

[100] W. Van Gijn, P. Krijnen, V. Lemmens, M. Den Dulk, H. Putter, and C. van de Velde, "Quality assurance in rectal cancer treatment in the netherlands: A catch up compared to colon cancer treatment," *European Journal of Surgical Oncology (EJSO)*, vol. 36, no. 4, pp. 340–344, 2010.

[101] W. H. Organization *et al.*, *Quality assurance in radiotherapy: a guide prepared following a workshop held at Schloss Reisensburg, Federal Republic of Germany, 3-7 December 1984*. World Health Organization, 1988.

[102] G. J. Kutcher, L. Coia, M. Gillin, *et al.*, "Comprehensive qa for radiation oncology: Report of aapm radiation therapy committee task group 40," *MEDICAL PHYSICS-LANCASTER PA-*, vol. 21, pp. 581–581, 1994.

[103] K. Vergote, Y. De Deene, W. Duthoy, *et al.*, "Validation and application of polymer gel dosimetry for the dose verification of an intensity-modulated arc therapy (imat) treatment," *Physics in Medicine & Biology*, vol. 49, no. 2, p. 287, 2004.

[104] R. A. Siochi, P. Balter, C. D. Bloch, *et al.*, "A rapid communication from the aapm task group 201: Recommendations for the qa of external beam radiotherapy data transfer. aapm tg 201: Quality assurance of external beam radiotherapy data transfer," *Journal of applied clinical medical physics*, vol. 12, no. 1, pp. 170–181, 2011.

[105] M. M. Paulides, D. B. Rodrigues, G. G. Bellizzi, *et al.*, "Esho benchmarks for computational modeling and optimization in hyperthermia therapy," *International Journal of Hyperthermia*, vol. 38, no. 1, pp. 1425–1442, 2021.

[106] R. Canters, M. Franckena, M. Paulides, and G. Van Rhoon, "Patient positioning in deep hyperthermia: Influences of inaccuracies, signal correction possibilities and optimization potential," *Physics in Medicine & Biology*, vol. 54, no. 12, p. 3923, 2009.

[107] M. H. Seegenschmiedt, P. Fessenden, and C. C. Vernon, *Thermoradiotherapy and Thermochemotherapy: Biology, Physiology, Physics*. Springer, 1995, vol. 1.

[108] R. J. Myerson, E. G. Moros, C. J. Diederich, *et al.*, "Components of a hyperthermia clinic: Recommendations for staffing, equipment, and treatment monitoring," *International Journal of Hyperthermia*, vol. 30, no. 1, pp. 1–5, 2014.

[109] P. Wust, H. Fähling, R. Felix, *et al.*, "Quality control of the sigma applicator using a lamp phantom: A four-centre comparison," *International journal of hyperthermia*, vol. 11, no. 6, pp. 755–768, 1995.

[110] S. Curto, H. T. Mulder, B. Aklan, *et al.*, "A multi-institution study: Comparison of the heating patterns of five different mr-guided deep hyperthermia systems using an anthropomorphic phantom," *International Journal of Hyperthermia*, vol. 37, no. 1, pp. 1103–1115, 2020.

[111] H. T. Mulder, S. Curto, M. M. Paulides, M. Franckena, and G. C. van Rhoon, "Systematic quality assurance of the bsd2000-3d mr-compatible hyperthermia applicator performance using mr temperature imaging," *International Journal of Hyperthermia*, vol. 35, no. 1, pp. 305–313, 2018.

[112] R. Canters, P. Wust, J. Bakker, and G. Van Rhoon, "A literature survey on indicators for characterisation and optimisation of sar distributions in deep hyperthermia, a plea for standardisation," *International Journal of Hyperthermia*, vol. 25, no. 7, pp. 593–608, 2009.

[113] P. Wust, H. Fähling, A. Jordan, J. Nadobny, M. Seebass, and R. Felix, "Development and testing of sar-visualizing phantoms for quality control in rf hyperthermia," *International journal of hyperthermia*, vol. 10, no. 1, pp. 127–142, 1994.

[114] P. Nilsson, "Physics and technique of microwave-induced hyperthermia in the treatment of malignant tumours.," Ph.D. dissertation, University of Lund, 1984.

[115] K. Ito, K. Furuya, Y. Okano, and L. Hamada, "Development and characteristics of a biological tissue-equivalent phantom for microwaves," *Electronics and Communications in Japan (Part I: Communications)*, vol. 84, no. 4, pp. 67–77, 2001.

[116] J. Lagendijk and P. Nilsson, "Hyperthermia dough: A fat and bone equivalent phantom to test microwave/radiofrequency hyperthermia heating systems," *Physics in medicine & biology*, vol. 30, no. 7, p. 709, 1985.

[117] H. D. Trefná, S. L. Navarro, F. Lorentzon, T. Nypelö, and A. Ström, "Fat tissue equivalent phantoms for microwave applications by reinforcing gelatin with nanocellulose," *Biomedical Physics & Engineering Express*, vol. 7, no. 6, p. 065 025, 2021.

[118] S. Allen, G. Kantor, H. Bassen, and P. Ruggera, "Quality-assurance reports: Cdrh rf phantom for hyperthermia systems evaluations," *International Journal of Hyperthermia*, vol. 4, no. 1, pp. 17–23, 1988.

[119] Y. Nikawa, M. Chino, and K. Kikuchi, "Soft and dry phantom modeling material using silicone rubber with carbon fiber," *IEEE transactions on microwave theory and techniques*, vol. 44, no. 10, pp. 1949–1953, 1996.

[120] J. Garrett and E. Fear, "Stable and flexible materials to mimic the dielectric properties of human soft tissues," *IEEE Antennas and Wireless Propagation Letters*, vol. 13, pp. 599–602, 2014.

[121] P. Hasgall, F. Di Gennaro, C. Baumgartner, *et al.*, "It'is database for thermal and electromagnetic parameters of biological tissues. version 4.0, 2018," *DOI: https://doi. org/10.13099/VIP21000-04-0. itis. swiss/database*, 2022.

[122] P. M. Meaney, C. J. Fox, S. D. Geimer, and K. D. Paulsen, "Electrical characterization of glycerin: Water mixtures: Implications for use as a coupling medium in microwave tomography," *IEEE transactions on microwave theory and techniques*, vol. 65, no. 5, pp. 1471–1478, 2017.

[123] M. De Lazzari, W. Napieralski, T. Nguyen, A. Ström, and H. D. Trefná, "Design and manufacture procedures of phantoms for hyperthermia qa guidelines," in *2023 17th European Conference on Antennas and Propagation (EuCAP)*, IEEE, 2023, pp. 1–5.

[124] M. M. Paulides, J. F. Bakker, A. P. Zwamborn, and G. C. Van Rhoon, "A head and neck hyperthermia applicator: Theoretical antenna array design," *International journal of hyperthermia*, vol. 23, no. 1, pp. 59–67, 2007.

[125] P. Takook, M. Persson, J. Gellermann, and H. D. Trefná, "Compact self-grounded bow-tie antenna design for an uwb phased-array hyperthermia applicator," *International Journal of Hyperthermia*, vol. 33, no. 4, pp. 387–400, 2017.

[126] C. Carrapiço-Seabra, M. De Lazzari, A. Ameziane, G. C. van Rhoon, H. Dobšıcek Trefná, and S. Curto, "Application of the esho-qa guidelines for determining the performance of the lca superficial hyperthermia heating system," *International Journal of Hyperthermia*, vol. 40, no. 1, p. 2 272 578, 2023.